AD-A140 478 COHERENT STRUCTURE MODELING OF VISCOUS SUBLAYER TURBULENCE FOR INCOMPRESS..(U) STANFORD UNIV CA DEPT OF AERONAUTICS AND ASTRONAUTICS D K OTA ET AL. FEB 84 1/1

UNCLASSIFIED SUDAA-AA-CFD-84-1 AFOSR-TR-84-0248 F/G 20/4 NL

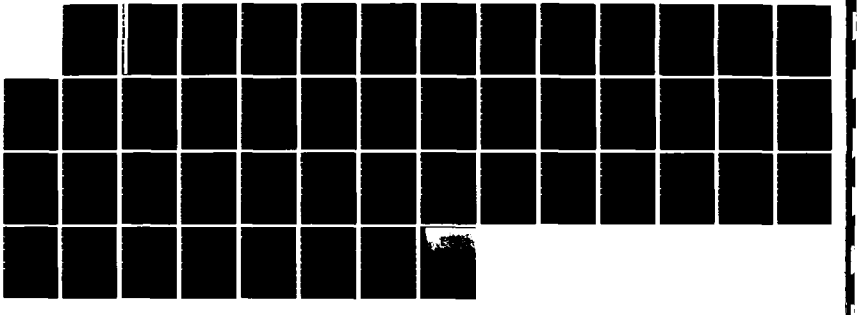

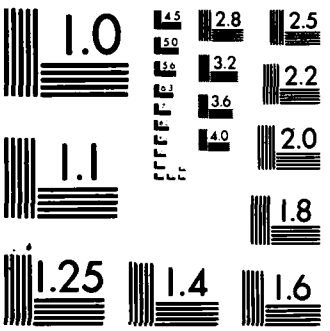

Department of AERONAUTICS and ASTRONAUTICS
STANFORD UNIVERSITY

Report AA CFD 84-1

SECOND ANNUAL SCIENTIFIC REPORT

January 1, 1983 to December 31, 1983

Air Force Office of Scientific Research Contract 81-NA-256

AFOSR-82-0083

COHERENT STRUCTURE MODELING OF VISCOUS SUBLAYER TURBULENCE FOR INCOMPRESSIBLE FLOW WITH HEAT TRANSFER AND FOR COMPRESSIBLE FLOW

BY

DALE K. OTA AND DEAN R. CHAPMAN

Submitted to the

Directorate of Aerospace Sciences
Air Force Office of Scientific Research
Bolling AFB
Washington D.C. 20332

by the

Department of Aeronautics and Astronautics
Stanford University
Stanford, CA 94305-2186

February 1984

Report AA CFD 84-1

SECOND ANNUAL SCIENTIFIC REPORT

January 1, 1983 to December 31, 1983

Air Force Office of Scientific Research Contract 81-NA-256

COHERENT STRUCTURE MODELING OF VISCOUS SUBLAYER TURBULENCE FOR INCOMPRESSIBLE FLOW WITH HEAT TRANSFER AND FOR COMPRESSIBLE FLOW

BY

DALE K. OTA AND DEAN R. CHAPMAN

Submitted to the

Directorate of Aerospace Sciences

Air Force Office of Scientific Research

Bolling AFB

Washington D.C. 20332

by the

Department of Aeronautics and Astronautics

Stanford University

Stanford, CA 94305-2186

February 1984

UNCLASSIFIED

SECURITY CLASSIFICATION OF THIS PAGE *(When Data Entered)*

REPORT DOCUMENTATION PAGE		READ INSTRUCTIONS BEFORE COMPLETING FORM
1. REPORT NUMBER **AFOSR-TR- 34-0248**	2. GOVT ACCESSION NO. AD-A140 478	3. RECIPIENT'S CATALOG NUMBER
4. TITLE *(and Subtitle)* Coherent Sturcture Modeling of Viscous Sublayer Turbulence for Incompressible Flow with Heat Transfer and for Compressible Flow		5. TYPE OF REPORT & PERIOD COVERED Second Annual Scientific Rpt. Jan. 1, 1983 to Dec. 31, 1983
		6. PERFORMING ORG. REPORT NUMBER
7. AUTHOR(s) Dale K. Ota and Dean R. Chapman		8. CONTRACT OR GRANT NUMBER(s) AFOSR 82-0083
9. PERFORMING ORGANIZATION NAME AND ADDRESS Department of Aeronautics and Astronautics Stanford University Stanford, CA 94305 -2186		10. PROGRAM ELEMENT, PROJECT, TASK AREA & WORK UNIT NUMBERS 61102 F 2307/A2
11. CONTROLLING OFFICE NAME AND ADDRESS Directorate of Aerospace Sciences (NA) Air Force Office of Scientific Research Bolling AFB, Washington, D.C. 20332		12. REPORT DATE February 1984
		13. NUMBER OF PAGES 44
14. MONITORING AGENCY NAME & ADDRESS(if different from Controlling Office)		15. SECURITY CLASS. (of this report) UNCLASSIFIED
		15a. DECLASSIFICATION/DOWNGRADING SCHEDULE

16. DISTRIBUTION STATEMENT *(of this Report)*

Approved for public release
distribution unlimited.

17. DISTRIBUTION STATEMENT *(of the abstract entered in Block 20, if different from Report)*

18. SUPPLEMENTARY NOTES

19. KEY WORDS *(Continue on reverse side if necessary and identify by block number)*

Fluid Mechanics, heat transfer, turbulent Prandtl number, viscous sublayer, Navier-Stokes, Computational Model

20. ABSTRACT *(Continue on reverse side if necessary and identify by block number)*

The general objective of the present research is to develop a Navier-Stokes computational model of the time-dependent dynamics and heat transfer in a compressible viscous sublayer. The main objective is to compute the variation of turbulent Prandtl number across the sublayer. Experiments have been unable to define this variation, and existing theories differ greatly. -

(continued on reverse)

DD FORM 1 JAN 73 1473

UNCLASSIFIED

SECURITY CLASSIFICATION OF THIS PAGE *(When Data Entered)*

(20. continued)

A computational code has been developed using preliminary, relatively simple temperature and velocity boundary conditions at the outer edge of the sublayer. Computations have been made for molecular Prandtl numbers from 0.7 to 6 with zero pressure gradient, and for adverse, zero, and favorable pressure gradient, with a Prandtl number of 0.7. These preliminary results show a strong effect of molecular Prandtl number on turbulent Prandtl number near the wall; but only a relatively small effect of pressure gradient throughout the sublayer. Future computations will be made with more refined boundary conditions.

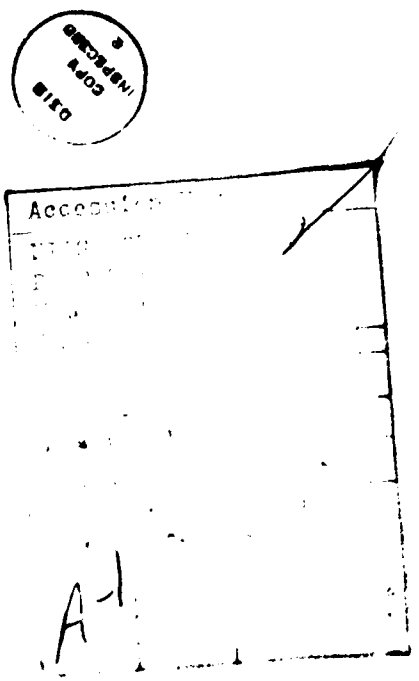

INTRODUCTION AND OBJECTIVES

Practical applications of computational fluid dynamics within the foreseeable future must necessarily utilize some form of turbulence modeling. Computations based on the Reynolds–averaged equations of motion require all turbulence transport of momentum and energy to be modeled; while large–eddy simulations require the subgrid–scale turbulence to be modeled. In both cases, the uncertainties in modeling turbulence within the viscous sublayer constitute a major weak link in the overall numerical computation.

During the past two decades a great deal of new experimental information has been assembled on the physics of organized eddy structures in turbulent flow, especially within the viscous sublayer (see, for example, the recent review of Cantwell, 1981). Yet it has not been possible thus far to incorporate this body of physical information within the framework of Reynolds–averaged turbulence modeling. The reason is fundamental, reflecting a well–known limitation in the Reynolds–average approach which begins by time averaging the dynamic equations of motion. In this initial mathematical step important physical aspects of organized eddy structures, such as phase relationships and coherent structure dynamics, are obliterated irreversibly. Consequently, some totally different approach is required if the observed physics of coherent eddy motions are to be incorporated within the framework of a turbulence model.

Quite recently a new approach has been developed for modeling viscous sublayer turbulence in incompressible flow without heat transfer (Chapman and Kuhn (1981). Their method models directly the essential organized eddy structures observed in experiments. The principal steps in this "coherent–structure modelling" are: first, to model velocity boundary conditions at the outer edge of the viscous sublayer, then to compute time–dependent dynamics, and finally to time average computed results. Thus, time averaging is the last operation performed on computed dynamics, rather than the first operation performed on the dynamic equations. This initial effort, although far from fully developed, already has been surprisingly successful in modeling some important characteristics

of viscous sublayer turbulence.

The over all objective of the present research is to develop, using the Navier–Stokes equations, a computational model of viscous sublayer turbulence applicable to flow with heat transfer and to compressible flow. Specific tasks within this objective are to utilize the model to compute the distribution of turbulent Prandtl number within the viscous sublayer (a) for fluids of various molecular Prandtl number, and (b) for flows with adverse, zero, and favorable streamwise pressure gradients.

Navier-Stokes computations of the turbulent Prandtl number Pr_t are significant because experimental techniques have been unable to provide reliable measurements within the viscous sublayer. This parameter, of course, affects turbulent heat transfer. Since by definition,

$$Pr_t = \frac{(\overline{uv})\left(\frac{\partial\bar{\theta}}{\partial y}\right)}{(\overline{\theta v})\left(\frac{\partial\bar{U}}{\partial y}\right)}$$

an experimental determination would require accurate measurements near a wall of the Reynolds stress $\overline{uv}$, the correlation $\overline{\theta v}$ between temperature θ and normal velocity, the mean velocity gradient $\partial\overline{U}/\partial y$, and the mean temperature gradient $\partial\bar{\theta}/\partial y$. To date, it has not been possible to make reliable measurements of these four quantities in the viscous sublayer. The band of uncertainty from one set of data for air (Simpson et al. (1970)), is illustrated in fig. 1. Other sets of experimental data, e.g. Fulachier (1972), indicate that the overall uncertainty band is even broader than this one set of measurements would indicate. Experiments are unable to determine whether the values of Pr_t near a wall are large, small, or intermediate. Experiments also have not been able to define how Pr_t varies with molecular Pr or with pressure gradient within the viscous sublayer. We believe that Navier–Stokes computations can shed much light on these uncertainties.

MOTIVATIONS FOR COHERENT STRUCTURE MODELING OF VISCOUS SUBLAYER TURBULENCE

Coherent–structure modeling departs markedly from Reynolds–averaging modeling, and thereby offers the potential of some entirely new advances in turbulence computation. Both the motivations and the payoff for this type of research are quite different from those for more conventional turbulence modeling. In addition to the specific motivations outlined above for the objectives of the present research, there are other important motivations that will affect different areas of turbulence computation. It is appropriate, therefore, to outline some of these.

Three other motivations for developing a realistic coherent-structure model of viscous sublayer turbulence are:

1 - *To provide a basis for strengthening a major weak link in present Reynolds–average closure schemes.* Conventional turbulence closure methods (e.g. $k-\epsilon$, other 2–equation methods, and Reynolds–Stress transport methods) all employ differential transport equations that are "modeled" forms of exact transport equations. The exact equation for the transport of dissipation, for example, contains very complex turbulence terms involving pressure–velocity correlations, triple correlations of velocity gradients, correlations of second derivatives of velocity, and correlations between pressure gradient and velocity gradient. Such correlations are not measurable with present experimental technology. Because modeled equations for free turbulence yield demonstrably incorrect results near a wall, various *ad hoc* functions (up to 5 in number) are added in an effort to mend this shortcoming. Without any guide or test basis from experiment, the inevitable consequence is that different models with different ad hoc functions yield different results for technically important quantities such as skin friction in flows with pressure gradient (Patel et. al 1981). If, however, a *realistic* Navier–Stokes computational model were developed for the time dependent dynamics of viscous sublayer flow, then all the terms in the exact transport equations could be computed. When compared

with corresponding modeled terms, a rational formulation would be obtained of the wall damping functions for integrating turbulence models across the viscous sublayer. This would strengthen a weak link in conventional turbulence models. Reynolds-average modeling, of course, will be the mainstay of practical turbulent flow computation for years to come.

2 - *To provide a simple test flow against which subgrid scale models of turbulence in large eddy simulations can be tested.* The simple flow of homogeneous shear, for example, computed in detail from the time-dependent Navier-Stokes equations (Rogallo 1977) has been used effectively as a test flow for assessing subgrid scale turbulence models for application in the outer region of a turbulent boundary layer or in free shear layers (e.g., Clark et. al. 1979, McMillan and Ferziger 1979, Shirani 1981). A realistic coherent-structure model of viscous sublayer turbulence, likewise computed from the time-dependent Navier-Stokes equations, could similarly be used to test subgrid-scale models for large eddy simulations of turbulent flow in the region adjacent to a wall.

3 - *To provide a guide for modeling the lower boundary conditions for the outer turbulent region in large eddy simulations of boundary layer flow.* If a realistic boundary condition of this type could be developed, the entire viscous sublayer could be modeled rather than directly computed. The required computer power for large eddy simulations at high Reynolds numbers would thereby be reduced by a very large factor (about 10^3; Chapman, 1980).

In summary of the motivations for developing coherent-structure turbulence models, it is clear that the potential payoffs are significant and of much broader scope than the specific objectives of the present research.

FORMULATION OF COMPUTATIONAL MODEL

DIFFERENTIAL EQUATIONS

The numerical scheme selected to solve the Navier–Stokes equations is an adaptation of the Pulliam and Steger (1980) code for compressible flow. Velocities in the physical x, $\bar{y}$, $\bar{z}$ domain are u, $\bar{v}$, $\bar{w}$. In the computational ξ, η, ς, domain the dependent variables are ρ, ρu, $\rho\bar{v}$, $\rho\bar{w}$, and $\rho\left[e_i + \left(u^2 + \bar{v}^2 + \bar{w}^2\right)/2\right]$, where e_i is the internal energy per unit mass. Pulliam and Steger use $\bar{z}$ as the coordinate normal to the surface, and $\bar{y}$ as the spanwise coordinate. In order to minimize code changes, we use this coordinate system in the numerical computations and then, at the end, change $\bar{z}$ to y, $\bar{w}$ to v, $\bar{y}$ to z, and $\bar{v}$ to w in order to present results in the more familiar boundary layer coordinate designations. We employ simple cartesian coordinates in the streamwise x– and spanwise $z = \bar{y}$–directions, and a stretched mesh in the normal $y = \bar{z}$ direction in order to concentrate points both near the wall and the outer edge. The metrics for the transformation are $\xi_x = 1$, $\eta_{\bar{y}} = 1/\Delta\bar{y}_+$, $\varsigma_{\bar{z}} = 1/\Delta\bar{z}_+$ where $\Delta\bar{y}_+$ and $\Delta\bar{z}_+$ are the mesh spacings in wall units in the spanwise and normal directions respectively.

The same basic physical approximation is made as in Chapman and Kuhn (1981), namely, that coherent sublayer eddy structures are highly elongate streamwise. In our case we assume–in accordance with experimental observations (e.g. Iritani et. al (1981)) — that the temperature eddies are also highly elongate streamwise. In the notation of Pulliam and Steger, the corresponding divergence form of the Navier–Stokes equations is

$$\partial_t \hat{q} = \partial_\eta(\hat{F}_v - \hat{F}) + \partial_\varsigma(\hat{G}_v - \hat{G}) + \hat{F}_p \tag{1}$$

where the vectors $\hat{F}$, $\hat{F}_v$, $\hat{G}$, $\hat{G}_v$ and $\hat{q}$ are identical to the conventional ones used by Pulliam and Steger for the case of orthogonal coordinates corresponding to the metrics of equation

(1). However, the vector

$$\hat{F}_p = J^{-1} \begin{bmatrix} 0 \\ -\frac{\partial p_e}{\partial x} \\ 0 \\ -\frac{\partial p_e}{\partial x} \\ \frac{-\gamma}{\gamma-1}\left[u_e \frac{\partial p_e}{\partial x} + \frac{\partial}{\partial z}(p_e w)\right] \end{bmatrix} \tag{2}$$

differs from theirs due to our assumption of highly elongate eddies in the streamwise direction. Thus, streamwise derivatives other than the mean streamwise pressure gradient dp_e/dx are neglected relative to derivatives in the spanwise and normal directions.

This basic approximation, which involves computation of 3 velocity components in 2 space directions, has been variously termed "2.5D flow", or "slender turbulence theory", or "slender eddy theory."

Since Pulliam and Steger used the thin-layer form of the Navier-Stokes equations, we write, in order to retain a tridiagonal structure,

$$\begin{aligned} \frac{\partial(\hat{F}_v - \hat{F})}{\partial q} &\equiv \frac{\partial \hat{F}}{\partial q} = A_o + A_x \\ \frac{\partial(\hat{G}_v - \hat{G})}{\partial q} &\equiv \frac{\partial \hat{G}}{\partial q} = B_o + B_x \end{aligned} \tag{3}$$

where the matrices A_o and B_o contain no cross derivative terms, while A_x and B_x contain all such terms. The detailed structure of these matrices is given in Appendix I. Our basic factored algorithm becomes

$$\begin{aligned} (I - \frac{2}{3}h\delta_\eta A_o^n)(I - \frac{2}{3}h\delta_\zeta B_o^n)\Delta\hat{q}^{n+1} = \frac{2}{3}h\left[\delta_\eta F^n + \partial_\zeta G^n\right] + \frac{2}{3}h\partial_\eta A_x^n \Delta q^n \\ + \frac{2}{3}h\delta_\zeta B_x^n \Delta q^n + \frac{2}{3}h\hat{F}_p + \frac{1}{3}\Delta\hat{q}^n \end{aligned} \tag{4}$$

This differs from the Pulliam–Steger algorithm by the addition of the last four terms on the right hand side. Of these, the last one corresponds to a three–point backward Euler difference scheme for time derivatives (added for accuracy and stability reasons explained later); the next to last term corresponds to body pressure gradients imposed by the large scale eddies, while the third and fourth from last represent the additional terms required for the full Navier–Stokes equations in place of the thin–layer equations used by Pulliam and Steger.

BOUNDARY CONDITIONS

The primary element in formulating our computational model involves the construction of time– and space–dependent boundary conditions that are as realistic as possible for the fluctuating temperature θ and the fluctuating velocity components u, v, w at the outer edge of the viscous sublayer. Various experimental observations are used as a guide to this construction. Computations using the time–dependent Navier–Stokes equations are then made over a length of time long enough for the various statistical quantities, e.g., mean values, correlation coefficients, rms fluctuating intensities, etc., to reach a periodic state within the viscous sublayer.

Our general approach is an extension of that employed by Chapman and Kuhn (1981) for incompressible flow without heat transfer. They considered two coherent components of turbulent motion at the outer edge of the viscous sublayer (lower edge of the logarithmic region). One component represents the small scale eddies (SSE) responsible for the principal production of turbulence and Reynolds stress. A second component represents the organized large scale eddies (LSE) which interact with the small scale eddies. They used a simple initial construction for purposes of illustrating the potential and main characteristics of this type of turbulence modeling. With all quantities expressed in conventional dimensionless wall variables, their velocity boundary conditions for the outer edge of the viscous sublayer were

Component 1–SSE		Component 2–LSE
$u_{e+} = 2\alpha_1 \sin N_1 T \sin\zeta$	+	$\sqrt{2(\alpha^2 - \alpha_1^2)}\sin(N_{u2}T + \phi_{u2})$
$v_{e+} = -2\beta \sin N_1 T \sin\zeta$		(5)
$w_{e+} = 2\beta \cos N_1 T \cos\zeta$	+	$\sqrt{\gamma^2 - \beta^2)}\sin(\frac{N_{u2}}{2}T + \phi_{w2})$

where α, β, γ are the rms intensities of fluctuation of u_{e+}, v_e, w_e, respectively, N_1 is the mean frequency of SSE burst events (ejection/sweep events), N_{u2} is the mean frequency of LSE, $\zeta \equiv 2\pi z/\lambda$ is a dimensionless spanwise distance variable, T is the dimensionless time, λ is the mean spacing between high-speed or low-speed streaks, α_1/α is the uv correlation coefficient (0.45), and ϕ_{u2} and ϕ_{w2} are phase angles. The flow model is periodic both in time and span. Hence the boundary conditions for the spanwise side walls of the computational domain were

$$\begin{aligned} u_{e+}(y,0,t) &= u_{e+}(y,\lambda,t) \\ v_{e+}(y,0,t) &= v_{e+}(y,\lambda,t) \\ w_{e+}(y,0,t) &= w_{e+}(y,\lambda,t) \end{aligned} \tag{6}$$

and at the surface

$$u_{e+}(0,z,t) = v_{e+}(0,z,t) = w_{e+}(0,z,t) = 0$$

This construction of velocity boundary conditions was guided by experimental observations of organized sublayer structure. For example, the $\sin\zeta$ factor for u_{e+} corresponds to the observation of high- and low-speed streaks spaced spanwise a mean distance of

λ apart, while the factors $\sin\zeta$, $\sin\zeta$, $\cos\zeta$ in the u_{e+}, v_{e+}, w_{e+} equations, respectively, correspond to a simple modeling of the observations of contra–rotating vortical motion near a wall. The 180 deg phase difference between u_{e+} and v_{e+} corresponds to observations from conditional samples in the sublayer that u and v are 180 deg out of phase during the Reynolds–stress intensive ejection–sweep event. The 90 deg phase difference in time between v_e and w_e corresponds to the observation that the derivative $(\partial\overline{v^2}/\partial y_+)_e$ at the outer edge of the viscous sublayer is zero. A comparison of a number of turbulence characteristics computed from this simple model with those measured in experiments showed surprisingly good agreement. This model was developed for flows with a mean streamwise pressure gradient, although numerical computations were made by Chapman and Kuhn only for the relatively small pressure gradients that exist in incompressible pipe and channel flow.

The above two–component velocity boundary conditions at the outer edge of the viscous sublayer are fully compatible with the concept of "active" and "inactive" components of turbulent motion in the log region as characterized by Townsend (1961) and Bradshaw (1967). Component 1 is active, involving small scale eddies, producing the Reynolds stress, being rotational, and being dependent on wall variables. Component 2 is inactive, involving large–scale eddies, producing energy but no Reynolds stress, being irrotational, and being dependent on outer variables. There is much experimental information that turbulent flow in the log region, and hence on the outer edge of the viscous sublayer, comprises these two distinct types of motion.

The computational model of Chapman and Kuhn is not regarded as sufficiently realistic for purposes such as outlined in the section above on motivations. Their results do illustrate, however, that the general approach employed has the potential of eventually leading to a sufficiently realistic model. Towards this end, it is believed that additional aspects of turbulence physics will have to be introduced into the model. For example, production of Reynolds stress should be intermittent in time, rather than sinusoidal–like as in boundary conditions (5). Also, conditional samples for $v(t)$ in ejection/sweep events

indicate that the v^2 turbulent energy contained in these SSE events should be only a fraction of the total v^2 energy, rather than the entire amount as in equation (5). Further, visualizations of viscous sublayer flow exhibit a mixture of order and disorder, rather than the coherent order only of equation (5). For the heat transfer case we must construct appropriate correspondingly boundary condition for the fluctuating temperature θ_e at the outer edge of the viscous sublayer.

One important guide to the construction of boundary conditions is provided by measurements of spectral density f. Fortunately, spectra for θ, u, v, and w, have been obtained by Fulachier (1972) at y-positions near the outer edge of the viscous sublayer. Data for $y_{e+} \approx 40$ (interpolated between his measurements at $y_+ = 31$ and 77) are shown in figure 2. Since

$$\int_0^\infty f dk = \int_0^\infty k f d(\ln k) = 1$$

the areas under curves of $u^2 k f_u$, $v^2 k f_v$, and $w^2 k f_w$ versus $\log k$ are proportional to the relative amounts of kinetic energy in these velocity components. Along the wave number scale k, pips are shown corresponding to LSE eddy scales of π/δ (where δ is the boundary layer thickness) and to SSE eddy scales of π/λ. It is seen that, whereas both u and θ exhibit eddy scales ranging from large $[O(\delta)]$ to small $[O(\lambda)]$, v exhibit scales ranging only from medium [O (several λ)] to small. Our boundary conditions will be constructed to be as consistent as possible with experimental data of this type.

A relatively simple method (developed under a separate contract) is used to simulate the intermittent character of Reynolds-stress production. Since $\overline{uv}$ is produced only by the active component of small scale eddies (SSE), only the time functions $\sin N_1 T$ and $\cos N_1 T$ in equation (1) need be modified. For this purpose we use a simple Fourier series approximation $H(\phi)$ to a rectangular pulse function, where $\phi \equiv N_1 T$.

For M terms in the approximating Fourier series, we have

$$H(\phi) = \sum_{1}^{M} (a_n \cos n\phi + b_n \sin n\phi)$$

$$\overline{H^2} = \frac{1}{2} \sum_{1}^{M} \left(a_n^2 + b_n^2\right) \tag{7}$$

$$a_n = \frac{1}{\pi n} \left[\sin nX_1 - \frac{X_1}{X_2} \sin nX_2\right]$$

$$b_n = \frac{1}{\pi n} \left[\frac{X_1}{X_2} (\cos nX_2 - 1) + (\cos nX_1 - 1)\right]$$

values of M in the range of 3 to 5 are anticipated. Initial computations will be made with $X_1 = X_2 = 0.25\pi$, since hot-wire measurements have indicated that the principal uv is produced in about 25% of the time, with relative uv quiescence the remaining 75% of time.

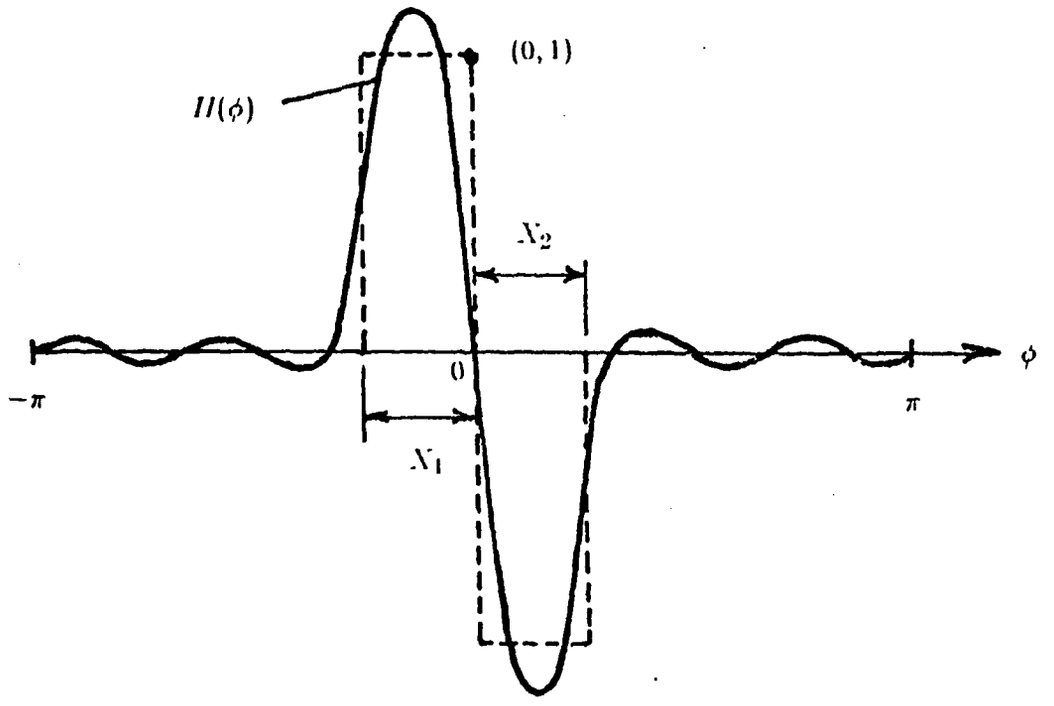

In conventional wall variables, the outer edge boundary conditions constructed to date include terms representing small scale eddies (SSE) of length scale λ, large scale eddies (LSE) of length scale $\geq 10\lambda$, and medium scale eddies (MSE) of intermediate length scale 3λ. Computations are made within a domain covering 3 spanwise cells each λ in width. The LSE are treated as being of sufficiently large scale that their time–dependent velocity component does not vary across the spanwise extent of the computational domain. The equation of continuity precludes having a LSE component in the boundary condition for v_e.

SSE	LSE	MSE
Scale λ	Scale $\geq 10\lambda$	Scale 3λ

$$
\begin{aligned}
u_e &= \sqrt{2}\alpha_1 F_u(\phi)\sin\zeta \quad + \sqrt{2(\alpha^2-\alpha_1^2)}\sin\left(N_{u2}T+\phi_{u2}\right) \\
v_e &= \sqrt{2}\beta_1 F_v(\phi)\sin\zeta \quad + 2\beta_2\sin\left(3N_{u2}T\right)\sin\frac{\zeta}{3} \\
w_e &= \sqrt{2}\beta_1 F_w(\phi)\cos\zeta \quad + \sqrt{2(\gamma^2-\beta_1^2)}\sin\left(\frac{N_{u2}}{2}T+\phi_{w2}\right)
\end{aligned}
\tag{8}
$$

$$
\theta_e = \sqrt{2}a_1 F_\theta(\phi)\sin\zeta + \sqrt{2(a^2-a_1^2)}\sin\left(N_{u2}T+\phi_{\theta 2}\right) \tag{9}
$$

where, in addition to the quantities already defined, $a \equiv \sqrt{(\overline{\theta^2})_e}$, $\phi_{\theta 2}$ is a phase angle in the large–eddy component of temperature, and

$$
\begin{aligned}
F_\theta(\phi) = -F_u(\phi) = F_v(\phi) &= \frac{H(\phi)}{\sqrt{H^2(\phi)}} \\
F_w(\phi) &= -\frac{H(\phi+\phi_{w1})}{\sqrt{H^2(\phi+\phi_{w1})}}
\end{aligned}
\tag{10}
$$

are the intermittent time functions normalized such that $\overline{F^2} = 1$. The boundary conditions for the spanwise side walls of the computational domain are

$$u_{e+}(y,0,t) = u_{e+}(y,3\lambda,t)$$
$$v_{e+}(y,0,t) = v_{e+}(y,3\lambda,t)$$
$$w_{e+}(y,0,t) = w_{e+}(y,3\lambda,t)$$

Thus the computation allows for flow interaction between the center cell and the two outside cells unconstrained by specific boundary conditions.

As in the model of Chapman and Kuhn: α, β, γ, a are determined from experimental data on the intensities of turbulence fluctuations in wall units at the outer edge of the viscous sublayer ($\alpha \approx 2, \beta \approx 1, \gamma \approx 1.3, a \approx 1.3$); ϕ_{w2}, $\phi_{\theta 2}$, ϕ_{u2}, are determined by computer trial to conform as well as possible to the mean–velocity law of the wall, mean–temperature law of the wall, and u–velocity skewness, respectively; ϕ_{w1} is determined analytically by the requirement that $(\partial\overline{v^2}/\partial y)_e$ is zero; α_1 is determined by the correlation coefficient $0.45 = -(R_{uv})_e = \alpha_1\beta_1/\alpha\beta$; a_1 is determined by the correlation coefficient $0.8 \approx -(R_{u\theta})_e = \frac{\alpha_1 a_1}{\alpha a} + \frac{1}{\alpha a}\sqrt{(\alpha^2-\alpha_1^2)(a^2-a_1^2)}\cos(\phi_{\theta 2} - \phi_{u2})$; and β_1/β is determined from conditional samples of the ejection/sweep event. This latter determination is made by assuming that the peak to peak amplitude *ratio* $< v >_{ppa} / < u >_{ppa}$, from the conditional samples is equal to the ratio β_1/α_1, and then using the above equation for $(R_{uv})_e$ to compute both β_1/β and α_1/α. An independent determination of α_1/α has been made from direct measurements of the fraction of total u^2 energy that exists during bursts, and hence also of β_1/β from the equation for $(R_{uv})_e$. Still a different determination has been made from $< w >_{ppa} / < u >_{ppa} = \beta_1/\alpha_1$ coupled with the equation for $(R_{uv})_e$.

Results of these determinations (made on a separate contract) are:

Data Source	Method	β_1/β
Chen & Balckwelder (1978)	$< v > / < u >$ plus $R_{uv} = -.45$	.53
Nakagawa & Nezu (1981)	$< v > / < u >$ plus $R_{uv} = -.45$	.72
Blackwelder & Kaplan (1979)	$< v > / < u >$ plus $R_{uv} = -.45$	.49
Kim (1982)	$< u > / < v >$ from LES computations, plus$R_{uv} = -.45$	.60
Kim, Kline & Reynolds (1971)	Fraction of total u^2 energy during bursts (.68), plus $R_{uv} = -.45$	.59
Blackwelder & Kaplan (1979)	$< w > / < u >$ plus $R_{uv} = -.45$	.64

On average, the value of β_1/β appears to be near 0.6.

It is to be noted that the structure of boundary conditions (8) comprises in equal proportions both ejection/sweep events (where a sweep follows an ejection), and sweep/ejection events (where an ejection follows a sweep). The recent experiments of Johansson and Alfredsson (1982) clearly reveal that both types of event occur. Their experimental VITA data for the smallest threshold values and the longest integration times employed, indicate these two event types to be about equally numerous. Both types have also been observed visually by Offen and Kline (1974) who use the term "cleansing sweep" in an ejection/sweep event to distinguish from sweeps in a sweep/ejection event.

STATUS OF RESEACH

I. Recapitulation of Research During 1982

During the first year of research, effort was directed mainly on surveying various existing theories for Pr_t in the viscous sublayer, on programming a Navier–Stokes code, and on testing and debugging this code.

Survey of various theories for Pr_t

Without a reliable guide from the experiment as to how Pr_t should be modeled near a wall, the various theoretical models advanced to date have differed greatly. This is illustrated in figures 3, 4, and 5 showing a compilation of various theories for fluids of molecular Prandtl number 0.72 (air), 6 (water), and 1000 (oil), respectively. These various theories are for zero pressure gradient and clearly demonstrate that a very wide range of uncertainty exists for Pr_t in the viscous sublayer. Present theories about the dependence of Pr_t on pressure gradient are fewer in number but also differ greatly.

Programming of Navier–Stokes Code

The implicit, compressible-flow, 3-D code of Pulliam and Steger (1980) has been used as the basic Navier–Stokes code to modify and adapt for viscous sublayer modeling. This code has been modified in five ways as follows: (1) the grid has been stretched to cluster points near the wall and the outer edge; (2) the flow variables have been made nondimensional in the conventional wall variables used for turbulent flows; (3) various necessary viscous terms have been added to bring the Pulliam–Steger "thin-layer" code into the full Navier–Stokes form; (4) the boundary conditions have been restructured to be appropriate for computations of viscous sublayer turbulence; (5) the algorithm for time derivatives has been revised for increased accuracy.

Testing and Debugging of Code

In order to test the algorithm accuracy for the time derivative terms, an exact analytical solution was derived for incompressible oscillating shear flow with heat transfer. This solution is an extension of the Chapman–Kuhn solution for flow without heat trans-

fer. Mathematical details of the analytical solution are presented in Appendix II. It was found that neither of the option algorithms in the original Pulliam–Steger code (i.e., Euler implicit first order, or trapezoidal second order) were sufficiently accurate for turbulence computations. With helpful guidance from Dr. Pulliam, a three–point backward Euler algorithm was coded and found to be satisfactory. The very close agreement obtained with this second–order accurate algorithm, between numerical computations and the exact analytical solution, is illustrated in figures 6 and 7 for the adiabatic–wall case and the heat–transfer case, respectively. Since oscillating shear flow with heat transfer involves viscous and heat–conduction terms as well as time–derivative terms, this test flow provides a check on the accuracy of the numeries for all three types of terms. It does not provide, however, a check on the accuracy of the important non–linear convection terms which are zero in oscillating shear flow.

Our initial runs of the viscous sublayer code revealed an instability problem associated with a large residual in the continuity equation, and a "decoupling" of the computed data in the y–direction normal to the wall. In this decoupling, computed values of $\bar{v}, \bar{p}$ and p' oscillated from grid point to grid point. Decoupling is usually a signal of a problem with boundary conditions. (This instability was minimized to acceptable levels by a coding change described below in the section on progress during 1983.) Examination of the continuity residual revealed that the instability arose at the outer edge of the viscous sublayer, since there the residual was around 10^{-1}, whereas in the inner main portion of the flow it was the order of 10^{-3} to 10^{-6}. This also suggests that the initial boundary conditions at the outer edge were creating a problem. Such problems can arise form either physical or numerical causes. Some trials with obviously wrong boundary conditions produced very extreme decoupling, leading to a blow up of the code.

II. Research Progress During 1983

During the past year, research has been focused on completing the programming, on investigating various types of boundary conditions, and on conducting some preliminary

computer runs to explore the effects on turbulent Prandtl number of variations in molecular Prandtl number and in mean streamwise pressure gradient.

Programming Modifications

Considerable code modification was undertaken in order to expand the data output and graphics program, to increase code robustness, and to transfer the code to two new computers installed at the Ames Research Center during 1983. The data output and associated graphics program was extended to handle 26 statistical quantities: the mean velocities $\bar{u}, \bar{v}, \bar{w}$, temperature $\bar{\theta}$, pressure $\bar{p}$ and density $\bar{\varsigma}$, the Reynolds stresses $\bar{uv}$, $\bar{uw}$ and velocity-temperature correlations $\bar{u\theta}, \bar{v\theta}$, the intensities of fluctuations u', v', w', θ', p', ς', $(uv)'$, the correlation coefficients R_{uv}, $R_{v\theta}$, $R_{u\theta}$, the skewness S_u, S_θ, S_{uv} and the flatness factors F_u, F_θ, F_{uv}. It was found that refinement of the grid from 25 x17 to 39 x 25 in the spanwise plane increased considerably the codes' robustness in handling a variety of boundary conditions that were explored. The finer grid apparently localizes boundary-condition problems near the outer edge of the viscous sublayer, and allows for a greater portion of the interior flow to be well behaved. Some tests were made of adding an artificial dissipation subroutine to the code in order to assess its effects on the stability and decoupling problems. Both stability and decoupling were improved, but the numerical results were altered considerably, and hence the artificial dissipation subroutine was dropped from further consideration.

During 1983 NASA Ames replaced the CDC 7600 computer, which we had originally programmed for, first by the CRAY--1S, and then later replaced this computer by the CRAY-XMP. The corresponding changes in operating system required some modifications to the code. To date all three of these computers have been used in the present research project.

Research on Boundary Conditions

In a code for 3-D compressible-viscous flow, five boundary conditions are required at every boundary. Not any combination of five conditions will work. This problem is

particularly acute at the out edge of our computational domain where non-zero velocity components are specified and where fluid flows in and out across this boundary. The set of boundary conditions which is physically and mathematically correct for this type of viscous compressible flow is not known a priori. Since no sound theoretical guide is available, considerable computer trial is necessary using various types of boundary conditions. Further complexity arises because the numerical boundary conditions can be treated either explicitly or implicitly. To date explicit boundary condition schemes have been mainly used. One implicit scheme has been tried, but has not provided an improvement in either accuracy or stability.

In the present research we have generalized the boundary conditions of Chapman and Kuhn (1981) who worked with incompressible flow. Difficult problems of boundary conditions arise when it is attempted to compute a compressible flow. If the dissipative terms were to dominate at the outer boundary, then a stable scheme would likely occur with the specification of velocities u_e, v_e, w_e, temperature θ_e, and either pressure p_e or density ρ_e. If the non-linear convective terms dominate, however, then this may only be weakly stable at best. Under such circumstances a characteristics type set of boundary conditions might have to be implemented. With Navier-Stokes codes the situation is not usually near either of these two extremes, but is somewhere in between. Specification of wrong boundary conditions can result in serious stability problems. In the present research we have attempted to structure boundary conditions that use as much as possible of the previous work of Chapman and Kuhn, and still provide adequate stability.

One change was found to be necessary to achieve stability. At the outer edge, the mass flux quantities $(\rho u)_e$, $(\rho w)_e$, $(\rho w)_e$ are specified instead of the velocity components. In this way mass is conserved within the computational domain. For the fourth boundary condition the outer-edge temperature θ_e has been modeled in a structural form similar to that of the u-component of velocity. For the fifth boundary condition at the outer edge of the viscous sublayer, there are a number of possibilities of which the following have been

investigated:

(a) p_e extrapolated from y–momentum equation

(b) ρ_e extrapolated from continuity equation

(c) $\rho_e = \bar{\rho}_e\,[1 + \epsilon \sin(N_1 T + \phi_1) + \delta \sin(N_1 T + \phi_2)]$

(d) $\rho_e = \bar{\rho}_e\,[1 + \epsilon \sin(N_1 T + \phi_1) + \delta \sin(N_1 T + \phi_2)]^{-1}$

(e) ρ_e extrapolated from $(\frac{\partial \rho}{\partial y})_e = 0$

It is noted that boundary conditions of the types (a) and (b) do not introduce any additional physical assumptions about the turbulence, and hence are the most desirable. Thus far, the most success has been obtained with conditions (a), and the numerical results presented later were obtained using this condition.

Two quite different types of boundary condition also have been explored wherein derivatives of velocity are modeled:

(f) $(\rho v)_e$, $(\rho w)_e$, θ_e specified with condition (a) and $(\frac{\partial u}{\partial y})_e = (\frac{\partial \bar{u}}{\partial y})_e[1+\epsilon \sin(N_1 T+\phi_1) \sin \xi + \delta \sin(N_1 T + \phi_2)]$

(g) $(\rho u)_e$, $(\rho v)_e$, $(\rho w)_e$ specified with condition (a) and $(\frac{\partial \theta}{\partial y})_e = (\frac{\partial \bar{\theta}}{\partial y})_e[1 + \epsilon \sin(N_1 T + \phi_1) \sin \xi + \delta \sin(N_1 T + \phi_2)]$

These two types of boundary conditions yielded somewhat more realistic values for the temperature intensity θ' and the fluctuating pressure intensity p'. Other quantities such as mean velocity $\bar{u}$ and mean temperature $\bar{\theta}$, however, were less realistic.

One further generalization in the structure of the outer–edge boundary conditions was coded in 1983. The Fourier series equations representing intermittent Reynolds stress production, equations (7) and (10), have been included in the computer program. Exploratory cases with this type of boundary condition will be run during 1984.

Preliminary Results for Various Pressure Gradients and Molecular Prandtl Number

Our computational results to date have been obtained with boundary conditions on $(\rho u/\bar{\rho})_e$, $(\rho v/\bar{\rho})_e$, $(\rho w/\bar{\rho})_e$ specified to be the same as Chapman–Kuhn (i.e., the same as the right hand side of equations (5)), with condition (a) above imposed, and with θ_e specified

as

$$\theta_e = 2a_1 \sin(N_1 T + \phi_{\theta 1}) \sin \xi + \sqrt{2(a^2 - a_1^2)} \sin(N_{u2} T + \phi_{\theta 2})$$

Here a is the intensity of temperature fluctuation at the outer edge ($a = 1.5$ in wall variables). The phase angles $\phi_{\theta 1}$, $\phi_{\theta 2}$, and the coefficient a_1 for these preliminary results were selected so that the $\bar{u\theta}$ correlation coefficient would be -0.8 at the outer edge and the $\bar{v\theta}$ correlation coefficient 0.45. These preliminary results serve to illustrate the type of results to be produced by our Navier–Stokes code, as well as the qualitative dependence of Pr_t on the parameters such as pressure gradient and molecular Pr.

In figure 8 a comparison is presented of our preliminary computations with experimental results for mean temperature $\bar{\theta}$, intensity of temperature fluctuation θ', and the two temperature–velocity correlation coefficients $R_{u\theta}$ and $R_{v\theta}$. These data are for air, $Pr = 0.7$, with zero pressure gradient and an isothermal wall. The computed mean temperature field and $R_{u\theta}$ agree well with experiment, but the computed temperature intensity and $R_{v\theta}$ are higher than experiment. Computed values of $R_{v\theta}$ are believed to be high because all of the modeled v energy in the boundary conditions of equation (5) is contained in the small scale eddy component which is correlated with the small scale eddy component of temperature. It is anticipated that use of a more realistic boundary condition for v_e, such as represented by equation (8), wherein only part of the v energy is contained in the correlated small scale component, will lower the computed $R_{v\theta}$ to values in closer agreement with experiment. Reasons for the relatively high values computed for temperature intensity are not understood at the present time. Further research with varied boundary conditions should clarify this.

Some computations have been made in order to provide a preliminary assessment of the effects of molecular Prandtl number Pr on the turbulent Prandtl number Pr_t in the viscous sublayer. Runs were conducted for $Pr = 0.7$, 1.5, 3, 6. Higher values of Pr encountered a stability problem which is being investigated. The computed results for an isothermal wall

are presented in figure 9. In some limited respects these results agree qualitatively with two of the various theories advanced to date, namely, the theories of Cebeci (1970) and Geshev (1978). The summary of various theories in figures 3, 4, and 5 include these two. It is interesting that the computed effect of Pr on Pr_t near the wall is opposite to that near the outer edge of the viscous sublayer. The computed curves intersect near $y_+ = 5$. Near the wall, our computed Pr_t increases considerably with Pr. Geshev's theory for an isothermal wall indicated a similar increase.

Values of Pr_t at $y_+ = 2$

Pr	Present Computation	Geshev	Cebeci
0.7	.98	.85	1.25
6.0	2.0	2.2	1.04

Other theories among those compiled in figures 3–5, however, do not indicate such a strong increase of Pr_t with increasing Pr near a wall; and Cebeci's theory indicates that Pr_t near the wall decreases with increasing Pr. It is noted that Geshev's treatment of wall temperature boundary condition is more realistic than the others, and affects $\overline{v\theta}$ and hence Pr_t near the wall in an important way. Near the outer edge of the viscous sublayer the effect of Pr on Pr_t is relatively small, as might be anticipated. The computed trend of $Pr_t > 1$ for $Pr < 1$ and $Pr_t < 1$ for $Pr > 1$ is consistent with experimental data. In this case Cebeci's theory indicates the same trend but Geshev's does not.

Values of Pr_t at $y_+ = 20$

Pr	Present Computation	Geshev	Cebeci
0.7	1.12	.95	1.16
6.0	.85	1.10	1.00

The various theories do not exhibit the near independence of Pr_t on Pr around $y_+ \approx 5$ that our preliminary computations exhibit.

Some preliminary computer runs were also made to explore the effects of mean streamwise pressure gradient on Pr_t for air ($Pr = 0.7$) flowing over an isothermal wall. In this

case the boundary conditions were the same as above, except that the bursting frequency N_1 of small scale eddies was changed with pressure gradient in accordance with the experimental data of Schraub and Kline (1965). The values selected for pressure gradient in wall variables were $d\bar{p}_+/dx_+ = -.02$ (favorable), 0, $+.02$ (adverse). As illustrated in figure 10, the computed results indicate relatively little effect of mean streamwise pressure gradient on Pr_t. In this case also the qualitative effect of $d\bar{p}/dx$ on Pr_t near the wall is opposite to that near the outer edge. Near the outer edge, the trend of increasing Pr_t with increasing favorable pressure gradient (decreasing $d\bar{p}/dx$) is qualitatively consistent with the trend deduced from experimental data (Blackwell (1972), Gibson (1981)). This trend is the opposite from that indicated by the recent theory of Thomas (1982). Below is a comparison of Pr_t values near the wall.

Values of Pr_t at $y_+ = 5$

$\frac{d\bar{p}_+}{dx_+}$	Present Computation	Thomas Theory	Blackwell Experiment
$-.02$	.95		
0	1.12	.85	1.80
$+.02$	1.12	1.00	1.60

Near the outer edge of the viscous sublayer the corresponding results are:

Values of Pr_t at $y_+ = 20$

$\frac{d\bar{p}_+}{dx_+}$	Present Computation	Thomas Theory	Blackwell Experiment
$-.02$	1.20		
0	1.12	.90	.85
$+.02$	1.00	1.10	.75

Unlike our computed results, neither the results of Thomas or of Blackwell exhibit the crossover and nearly common intersection near $y_+ \approx 12.5$ of the curves for various $d\bar{p}_+/dx_+$.

It is emphasized that, since our present quantitative results are preliminary and will likely change somewhat as the temperature and velocity boundary conditions are refined, the precise numerical values are not regarded as significant. The observed qualitative

trends, however, such as the strong increase near the wall of Pr_t with increasing Pr, and the relatively small effect of $d\bar{p}/dx$ on Pr_t, may not be markedly affected by such changes in these boundary conditions. These preliminary results serve to reveal mainly the types of information produced by the Navier–Stokes code being developed, and the qualitative trends which may not be altered as boundary conditions on temperature and velocity are further refined. If the preliminary result of only small effects of $d\bar{p}/dx$ on Pr_t holds up with more refined boundary conditions, this would be a simplifying and helpful result for practical computations of heat transfer. These preliminary results serve to illustrate the inconsistencies and deficiencies of the various theoretical models for Pr_t in the viscous sublayer.

III. Outline of Research Anticipated During 1984

Details of the research effort planned during 1984 have been given in our recent proposal dated July 1983 for continuation of the present research project. Very briefly, the main effort will be expended in the areas of: (1) refining the temperature boundary condition; (2) using more complex velocity boundary conditions such as those representing intermittent Reynolds stress productions; and those involving two components of v velocity; and (3), to the extent that time permits, investigating ways of further reducing the decoupling observed in $\bar{v}$, $\bar{p}$, and p' very near the wall, and ways of further improving the stability and robustness of the code.

REFERENCES

[1] Back, L. H., Cuffel, R. F., and Massier, P. F. (1970): Effect of Wall Cooling on the Mean Structure of a Turbulent Boundary Layer in Low-Speed Gas Flow. Int. J. Heat Mass Transfer, 13, pp. 1029–1047.

[2] Beam, R. M. and Warming, R. F. (1978): An Implicit Factored Scheme for the Compressible Navier–Stokes Equations. AIAA Journal, 16, pp. 393–402.

[3] Blackwell, B. F. (1972): The Turbulent Boundary Layer on a Porous Plate: An Experimental Study of the Heat Transfer Behavior with Adverse Pressure Gradients. Report HMT–16, Dept. of Mech. Eng., Stanford University.

[4] Blackwelder, R. F. and Kaplan, R. E. (1976): On the Wall Structure of the Turbulent Boundary Layer. Jour., Fluid Mech., 76, Pt. 1, pp 89–112.

[5] Bradshaw, P. (1967): "Inactive" Motions and Pressure Fluctuations in Turbulent Boundary Layers. Jour. Fluid Mech., 30, Pt. 2, pp 241–258.

[6] Cantwell, B.J. (1981): Organized Motion in Turbulent Flow. Ann. Rev. Fluid Mech., 13, pp 457–515.

[7] Cebeci, T. (1970): A Model for Eddy Conductivity and Turbulent Prandtl Number. Rept. No. MDC–J0747101, Douglas Aircraft Co., Long Beach, California.

[8] Chapman, D.R. (1980): Trends and Pacing Items in Computational Aerodynamics. Lecture Notes in Physics, Springer–Verlag, 141, pp. 1–11.

[9] Chapman, D.R. and Kuhn, G.D. (1981): Two–Component Navier–Stokes Computational Model of Viscous Sublayer Turbulence. AIAA paper 81–1024, Proc. 5th CFD Conference, Palo Alto, California.

[10] Chen, C.H. and Blackwelder, R. (1978): Large–Scale Motion in a Turbulent Boundary layer: A Study using Temperature Contamination. Jour. Fluid Mech., 89, Pt. 1, pp. 1-31.

[11] Clark, R.A., Ferziger, J.H. and Reynolds, W.C. (1979): Evaluation of Subgrid–Scale Models Using Accurately Simulated Turbulent Flow. Jour. Fluid Mech., 91, Pt. 1, pp. 1–16.

[12] Fulachier, L. (1972): Contribution a L'Etude des Analogies des Champs Dynamique et Thermique dans une Couche Limite Turbulent. Effet de L'Aspiration. Thesis, University of Provence, France.

[13] Elena, M. (1977): Etude Experimentale de la Turbulence Au Voisinage de la Paroi D'un Tube Legerement Chauffe. Int. J. Heat and Mass Transfer, 20, pp. 935–944.

[14] Geshev, P. I. (1978): Influence of Heat Conduction of the Wall on the Turbulent

Prandtl Number in the Viscous Sublayer. Inzhenerno– Fizicheskii Zhurnal, 35, pp. 292–296.

[15] Gibson, M. M., Verriopoulos, C. A. and Nagaro, Y. (1981): Measurements in the Heated Turbulent Boundary Layer on a Mildly Curved Convex Surface. Turbulent Shear FLow, Third International Symposium, pp. 80–89.

[16] Hishida, M. and Nagaro, Y. (1979): Structure of Turbulent Velocity and Temperature Fluctuations in Fully Developed Pipe Flow. Journal of Heat Transfer, 101, pp. 15–22.

[17] Iritani, Y., Kasagi, N. and Hirata, H. (1981): Transport Mechanism in a Turbulent Boundary Layer–Visualized Behavior or Wall Temperature by Liquid Crystal. Submitted to Trans. JSME (B).

[18] Jischa, M., and Rieke, H. B. (1979): About the Prediction of Turbulent Prandtl and Schmidt Numbers From Modeled Transport Equations. Int. J. Heat and Mass Transfer, 22, pp. 1547–1555.

[19] Johansson, A.V. and Alfredsson, P.H. (1982): On the Structure of Turbulent Channel Flow. Jour. Fluid Mech., 122, pp. 295–314.

[20] Johnk, R. E. and Hanratty, T. J. (1982): Temperature Profiles for Turbulent FLow of Air in a Pipe. Chem. Eng. Sci., 17, pp. 867–881.

[21] Kader, B. A. (1971): Temperature and Concentration Profiles in Fully Turbulent Boundary Layers. Int. J. Heat and Mass Transfer, 24, pp. 1541–1544.

[22] Kays, W. M. and Moffat, R. J. (1975): The Behavior of Transpired Turbulent Boundary Layers. Studies in Convection, Vol. 1, pp. 223–319.

[23] Kim, J. (1982): On the structure of Wall Bounded Turbulent Flows. Paper presented at Amer. Phys. Soc. Division of Fluid Dynamics Meeting, Rutgers Univ., Nov. 21-23, 1982.

[24] Kim, H. T., Kline, S. J. and Reynolds, W. C. (1971): The Production of Turbulence Near a Smooth Wall in a Turbulent Boundary Layer. Jour. Fluid Mech., 50, Pt. 1, pp. 133–160.

[25] McMillan, O. J. and Ferziger, J. H. (1979): Direct Testing of Subgrid–Scale Models. AIAA Paper 79-0072.

[26] Meek, R. L. and Baer, A. D. (1973): Turbulent Heat Transfer and the Periodic Viscous Sublayer. Int. J. Heat and Mass Transfer, 16, pp. 1385–1396.

[27] Nakagawa, H. and Nezu, I. (1981): Structure of Space–time Correlations of Bursting Phenomena in an Open Channel Flow, Jour. Fluid Mech., 104, pp. 1–43.

[28] Offen, G. R. and Kline, S. J. (1974): Combined Dye–Streak and Hydrogen–Bubble Visual Observations of a Turbulent Boundary Layer. Jour. Fluid Mech., 62, Pt. 2, pp. 223–239.

[29] Patel, V. C., Rodi, W. and Scheuerer, G. (1981): Evaluation of Turbulence Models for Near–Wall and Low–Reynolds Number Flows. Proc. Third Symposium on Turbulent Shear Flows, Sept. 9–11, 1981, pp. 1.1–1.8.

[30] Pulliam, T. H. and Steger, J. L. (1980): Implicit Finite Difference Simulations of Three–Dimensional Compressible Flow. AIAA Jour., 18, pp. 149–158.

[31] Reynolds, A. J. (1975): The Prediction of Turbulent Prandtl and Schmidt Numbers. Int. J. Heat and Mass Transfer, 18, pp. 1055–1069.

[32] Rogallo, R. (1977): An ILLIAC Program for the Numerical Simulation of Homogeneous Incompressible Turbulence. NASA TM NO. 73, 203.

[33] Schraub, F. A. and Kline, S. J. (1965): A Study of the Structure of the Turbulent Boundary Layer with and without Longitudinal Pressure Gradients. Thermosciences Div. Report MD–12, Stanford University.

[34] Shirani, E., Ferziger, J. H. and Reynolds, W. C. (1981): Mixing of a Passive Scalar in Isotropic and Sheared Turbulence. Report No. TF–15, Thermosciences Division, Dept. Mechanical Engineering, Stanford University.

[35] Simpson, R. L., Whitten, D G. and Moffat, R. J.: An Experimental Study of the Turbulent Prandtl Number of Air with Injection and Suction. Int. J. Heat and Mass Transfer, 13, pp. 125–143.

[36] Snijders, A. L., Koppius, A. M. and Nieuwvelt, C. (1983): An Experimental Determination of the Turbulent Prandtl Number in the Inner Boundary Layer for Air Flow over a Flat Plat. Int. J. Heat Mass Transfer, 26, pp. 425–431.

[37] Subramanian, C. S. and Antonia, R. A. (1981): Effect of Reynolds Number on a Slightly Heated Turbulent Boundary Layer. Int. J. Heat and Mass Transfer, 24, pp. 1833–1846.

[38] Thomas, L. C. (1982): A Turbulent Burst Model for Energy Transfer in the Wall Region. Heat Transfer 1982 Proc. of the Seventh Int. Heat Transfer Conf., Vol. 3, pp. 307–312.

[39] Thomas, L. C. and Benton, D. J. (1982): A Turbulent Burst Model for Boundary Layer Flows with Pressure Gradients. Heat Transfer 1982 Proc. of the Seventh Int. Heat Transfer Conf., Vol. 3, pp. 313–318.

[40] Townsend, A. A. (1961): Equilibrium Layers and Wall Turbulence. Jour. Fluid Mech., 11, pp. 97–120.

APPENDIX I

DECOMPOSITION MATRICES

The derivatives $\partial\hat{F}/\partial q$ and $\partial\hat{G}/\partial q$ are each decomposed into two matrices, one (subscript zero) that does not contain cross derivative terms, and another (subscript x) that contains all such terms.

$$\frac{\partial \hat{F}}{\partial q} = A_o + A_x$$

$$\frac{\partial \hat{G}}{\partial q} = B_o + B_x$$

where the matrix A_o is

$$A_o = -\begin{vmatrix} 0 & 0 & \eta_y & 0 & 0 \\ -u\eta_y v & \eta_y v & \eta_y u & 0 & 0 \\ \eta_y(\phi^2 - v^2) & -\eta_y(\gamma-1)u & -\eta_y v(\gamma-1) & -\eta_y(\gamma-1)w & \eta_y(\gamma-1) \\ -w\eta_y v & 0 & \eta_y w & \eta_y v & 0 \\ \eta_y v\left[2\phi^2 - \gamma\frac{e}{\rho}\right] & -(\gamma-1)u\eta_y v & \left\{\begin{matrix} -(\gamma-1)\eta_y v^2 + \\ \eta_y\left[\gamma\frac{e}{\rho} - \phi^2\right] \end{matrix}\right\} & -(\gamma-1)w\eta_y v & \gamma\eta_y v \end{vmatrix}$$

$$+J^{-1}\begin{vmatrix} 0 & 0 & 0 & 0 & 0 \\ -s_1\delta(u/\rho) & s_1\delta_\eta\left(\frac{1}{\rho}\right) & 0 & 0 & 0 \\ -s_2\delta_\eta(v/\rho) & 0 & s_2\delta_\eta\left(\frac{1}{\rho}\right) & 0 & 0 \\ -s_1\delta_\eta(w/\rho) & 0 & 0 & s_1\delta_\eta\left(\frac{1}{\rho}\right) & 0 \\ \left\{\begin{matrix} (s_5 - s_1)\delta_\eta\left[\frac{u^2+w^2}{\rho}\right] \\ +(s_5 - s_2)\,\delta_\eta\left(\frac{v^2}{\rho}\right) - s_5\delta_\eta\left(\frac{e}{\rho^2}\right) \end{matrix}\right\} & (s_1 - s_5)\delta_\eta\left(\frac{u}{\rho}\right) & (s_2 - s_5)\delta_\eta\left(\frac{v}{\rho}\right) & (s_1 - s_5)\delta_\eta\left(\frac{w}{\rho}\right) & s_5\delta_\eta\left(\frac{1}{\rho}\right) \end{vmatrix} J$$

$$\phi^2 = \frac{1}{2}(\gamma - 1)(u^2 + v^2 + w^2)$$

$$s_1 = \mu\eta_y^2 \qquad s_2 = \frac{4}{3}s_1 \qquad s_5 = \frac{\gamma}{Pr}s_1$$

$$J = \text{Jacobian} = \frac{1}{\Delta y_+ \Delta z_+}$$

and the matrix A_z is

$$A_z = J^{-1}\begin{vmatrix} 0 & 0 & 0 & 0 & 0 \\ 0 & 0 & 0 & 0 & 0 \\ -s_4\delta_\zeta\left(\frac{w}{\rho}\right) & 0 & 0 & s_4\delta_\zeta\left(\frac{1}{\rho}\right) & 0 \\ -s_3\delta_\zeta\left(\frac{v}{\rho}\right) & 0 & s_3\delta_\zeta\left(\frac{1}{\rho}\right) & 0 & 0 \\ \begin{Bmatrix} -s_3\left[\frac{w}{\rho}\delta_\zeta v + w\delta_\zeta\left(\frac{v}{\rho}\right)\right] \\ -s_4\left[\frac{v}{\rho}\delta_\zeta w + v\delta_\zeta\left(\frac{w}{\rho}\right)\right] \end{Bmatrix} & 0 & s_4\frac{1}{\rho}\delta_\zeta w + s_3 w\delta_\zeta\left(\frac{1}{\rho}\right) & s_4 v\delta_\zeta\left(\frac{1}{\rho}\right) + s_3\frac{1}{\rho}\delta_\zeta v & 0 \end{vmatrix} J$$

$$s_3 = \mu\eta_y\zeta_z$$

$$s_4 = -\frac{2}{3}s_3$$

The matrix B_o is

$$B_o = -\begin{vmatrix} \zeta_z w & 0 & 0 & \zeta_z & 0 \\ -u\zeta_z w & \zeta_z w & 0 & \zeta_z u & 0 \\ -v\zeta_z w & 0 & 0 & \zeta_z v & 0 \\ \zeta_z\phi^2 - w^2\zeta_z & -\zeta_z(\gamma-1)u & -\zeta_z(\gamma-1)v & -\zeta_z(\gamma-2)w & \zeta_z(\gamma-1) \\ \zeta_2 w\left[2\phi^2 - \gamma_\rho^e\right] & -(\gamma-1)u\zeta_z w & -(\gamma-1)v\zeta_z w & \zeta_z\left[\gamma_\rho^e - \phi^2 - (\gamma-1)w^2\right] & \gamma\zeta_z w \end{vmatrix} +$$

$$+J^{-1}\begin{vmatrix} 0 & 0 & 0 & 0 & 0 \\ -T_1\delta_\varsigma\left(\frac{u}{\rho}\right) & T_1\delta_\varsigma\left(\frac{1}{\rho}\right) & 0 & 0 & 0 \\ -T_1\delta_\varsigma\left(\frac{v}{\rho}\right) & 0 & T_1\delta_\varsigma\left(\frac{1}{\rho}\right) & 0 & 0 \\ -T_2\delta_\varsigma\left(\frac{w}{\rho}\right) & 0 & 0 & T_2\delta_\varsigma\left(\frac{1}{\rho}\right) & 0 \\ \begin{Bmatrix}(T_5-T_1)\delta_\varsigma\left(\frac{u^2+v^2}{\rho}\right) \\ +(T_5-T_1)\delta_\varsigma\left(\frac{w^2}{\rho}\right)-T_5\delta_\varsigma\left(\frac{e}{\rho^2}\right)\end{Bmatrix} & (T_1-T_5)\delta_\varsigma\left(\frac{u}{\rho}\right) & (T_1-T_5)\delta_\varsigma\left(\frac{v}{\rho}\right) & (T_2-T_5)\delta_\varsigma\left(\frac{w}{\rho}\right) & T_5\delta_\varsigma\left(\frac{1}{\rho}\right) \end{vmatrix} J$$

$$T_1 = \mu\varsigma_x^2 \qquad T_2 = \frac{4}{3}T_1 \qquad T_5 = \frac{\gamma}{Pr}T_1$$

and the matrix B_x is

$$B_x = J^{-1}\begin{vmatrix} 0 & 0 & 0 & 0 & 0 \\ 0 & 0 & 0 & 0 & 0 \\ -s_3\delta_\eta\left(\frac{w}{\rho}\right) & 0 & 0 & s_3\delta_\eta\left(\frac{1}{\rho}\right) & 0 \\ -s_4\delta_\eta\left(\frac{v}{\rho}\right) & 0 & s_4\delta_\eta\left(\frac{1}{\rho}\right) & 0 & 0 \\ \begin{Bmatrix}-s_3\left[\frac{v}{\rho}\delta_\eta w+v\delta_\eta\left(\frac{w}{\delta}\right)\right] \\ -s_4\left[\frac{w}{\rho}\delta_\eta v+w\delta_\eta\left(\frac{v}{\rho}\right)\right]\end{Bmatrix} & 0 & s_4 w\delta_\eta\left(\frac{1}{\rho}\right)+s_3\frac{1}{\rho}\delta_\eta w & s_3 v\delta_\eta\left(\frac{1}{\rho}\right)+s_4\frac{1}{\rho}\delta_\eta v & 0 \end{vmatrix} J$$

APPENDIX II

An exact analytical solution has been derived for oscillating shear flow with heat transfer in an incompressible fluid with constant properties. Since the momentum equations are independent of the thermal energy equation in incompressible flow, the velocity field is the same as for the case without heat transfer derived by Chapman and Kuhn (1981). With y as the coordinate normal to the infinite flat surface, and u and v as the velocity components in the streamwise and spanwise directions, respectively, we have

$$u = A\left[\sin nt - e^{-k_n y}\sin(nt - k_n y)\right] + cy$$

$$w = B\left[\sin(mt + (\phi) - e^{-k_m y}\sin(mt - k_m y)\right]$$

where

$$k_n = \sqrt{\frac{n}{2\nu}} \qquad k_m = \sqrt{\frac{m}{2\nu}}$$

The oscillating frequencies are n in the streamwise direction and m in the spanwise direction, and the mean velocity profile is $\bar{u} = cy$. For this velocity field, the solution to the thermal energy equation

$$\rho c_p \frac{\partial \theta}{\partial t} = k\frac{\partial^2 \theta}{\partial y^2} + \mu\left[\left(\frac{\partial u}{\partial y}\right)^2 + \left(\frac{\partial v}{\partial y}\right)^2\right]$$

is

$$\begin{aligned} T(z,t) = {} & B_1 y^2 + c_1 y + c_2 + B_e^{-2k_n y} + B_3 e^{-2k_m y} \\ & + A_2 e^{-k_n y}\left[\sin(nt - k_n y) - \cos(nt - k_n y)\right] - A_3 e^{-2k_n y}\cos 2(nt - k_n y) \\ & - A_4 e^{-2k_m y}\cos 2(mt + \phi - k_m y) - A_2 e^{-\beta_1 y}\sin(nt - \beta_1 y) \\ & - A_2 e^{-\beta_1 t}\cos(nt - \beta_1 y) + A_3 e^{-\beta_2 y}\cos(2nt - \beta_2 y) \\ & + A_4 e^{-\beta_3 y}\cos(2mt + 2\phi - \beta_3 y) \end{aligned}$$

$$\beta_1 = \sqrt{\frac{n}{2} Pr \frac{\rho}{\mu}} \qquad \beta_2 = \sqrt{nPr\frac{\rho}{\mu}} \qquad \beta_3 = \sqrt{mPr\frac{\rho}{\mu}}$$

$$B_1 = -\frac{Prc^2}{2C_p} \qquad A_2 = \frac{2Ack_n}{C_p Re\left(n - \frac{2k_n^2\mu}{\rho Pr}\right)}$$

$$B_2 = -A^2\frac{Pr}{4C_p} \qquad A_3 = \frac{A^2k_n^2}{C_p Re\left(2n - \frac{8k_n^2\mu}{\rho Pr}\right)}$$

$$B_3 = -\beta^2\frac{Pr}{4C_p} \qquad A_4 = \frac{B^2k_m^2}{C_p Re\left(2m - \frac{8k_m^2\mu}{\rho Pr}\right)}$$

$$C_1 = \frac{1}{y_e}\left[T_\infty - C_2 + \frac{Prc^2y_e^2}{2C_p}\right]$$

$$C_2 = T_w + \frac{Pr(A^2 + B^2)}{4C_p}$$

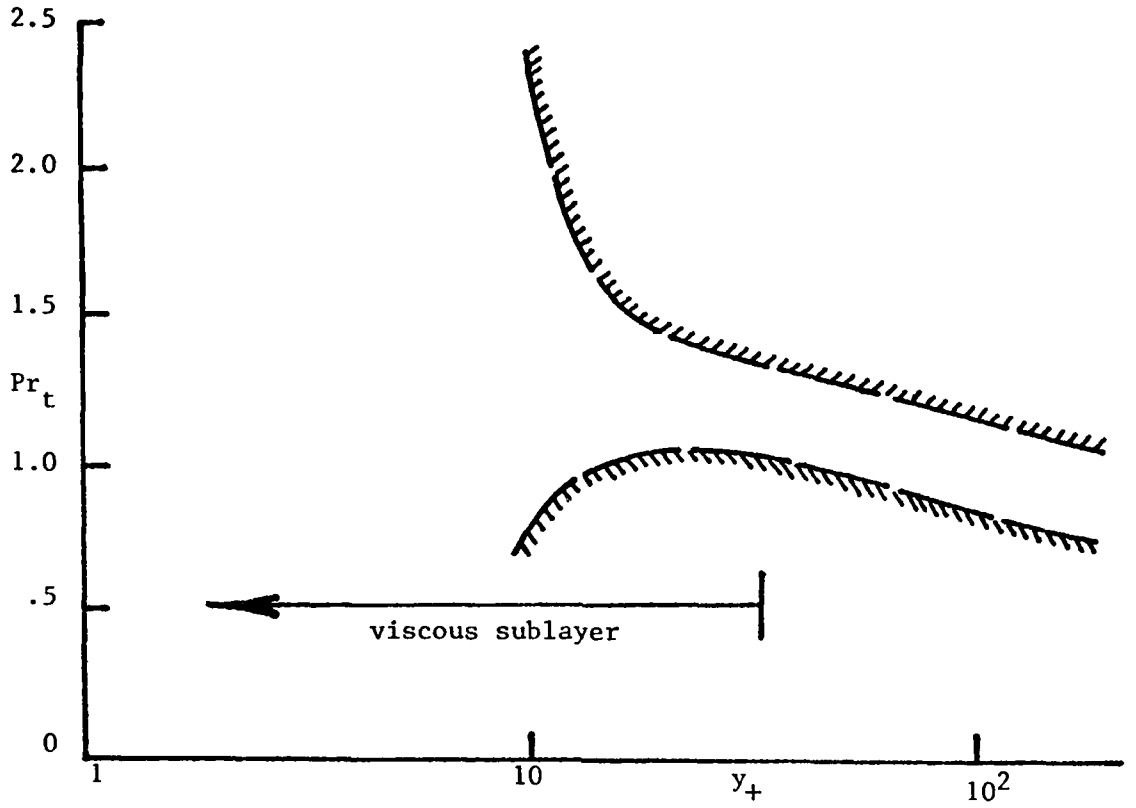

Figure 1. - Envelope of experimental uncertainty for turbulent Prandtl number from data of Simpson et. al. (1970).

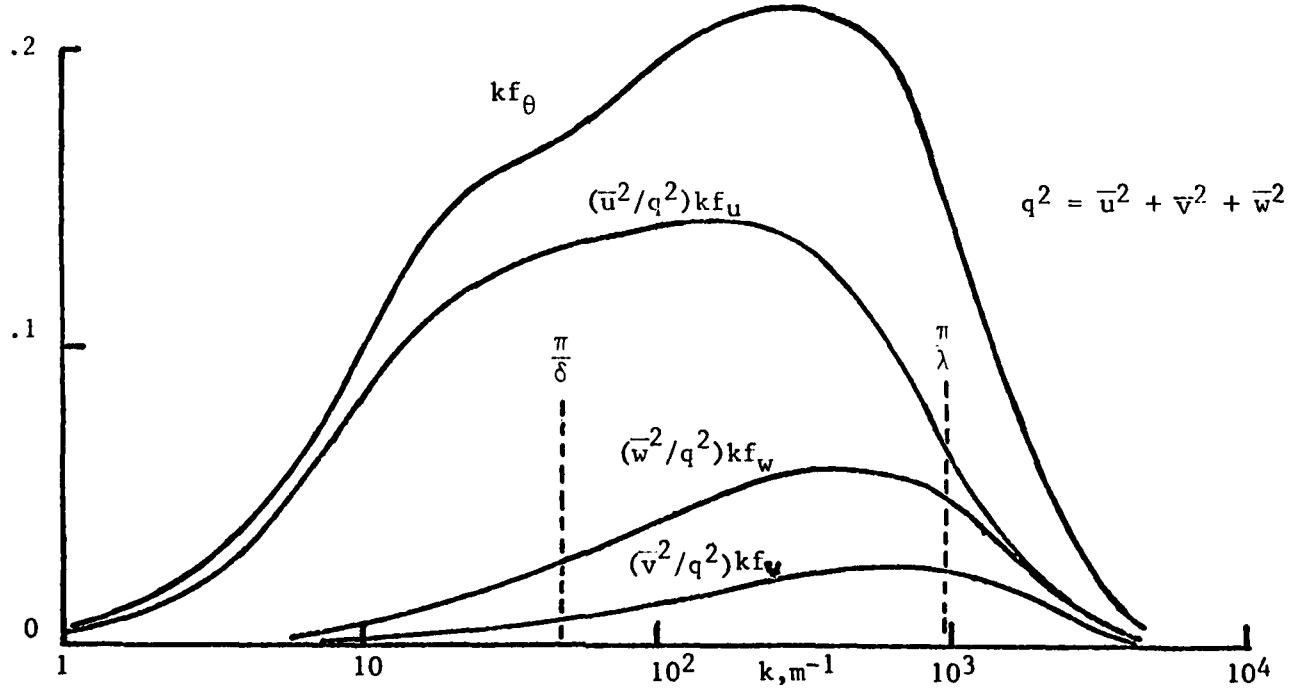

Figure 2. Spectral density of the three components of velocity fluctuation at $y_+ = 40$ from data of Fulachier (1972).

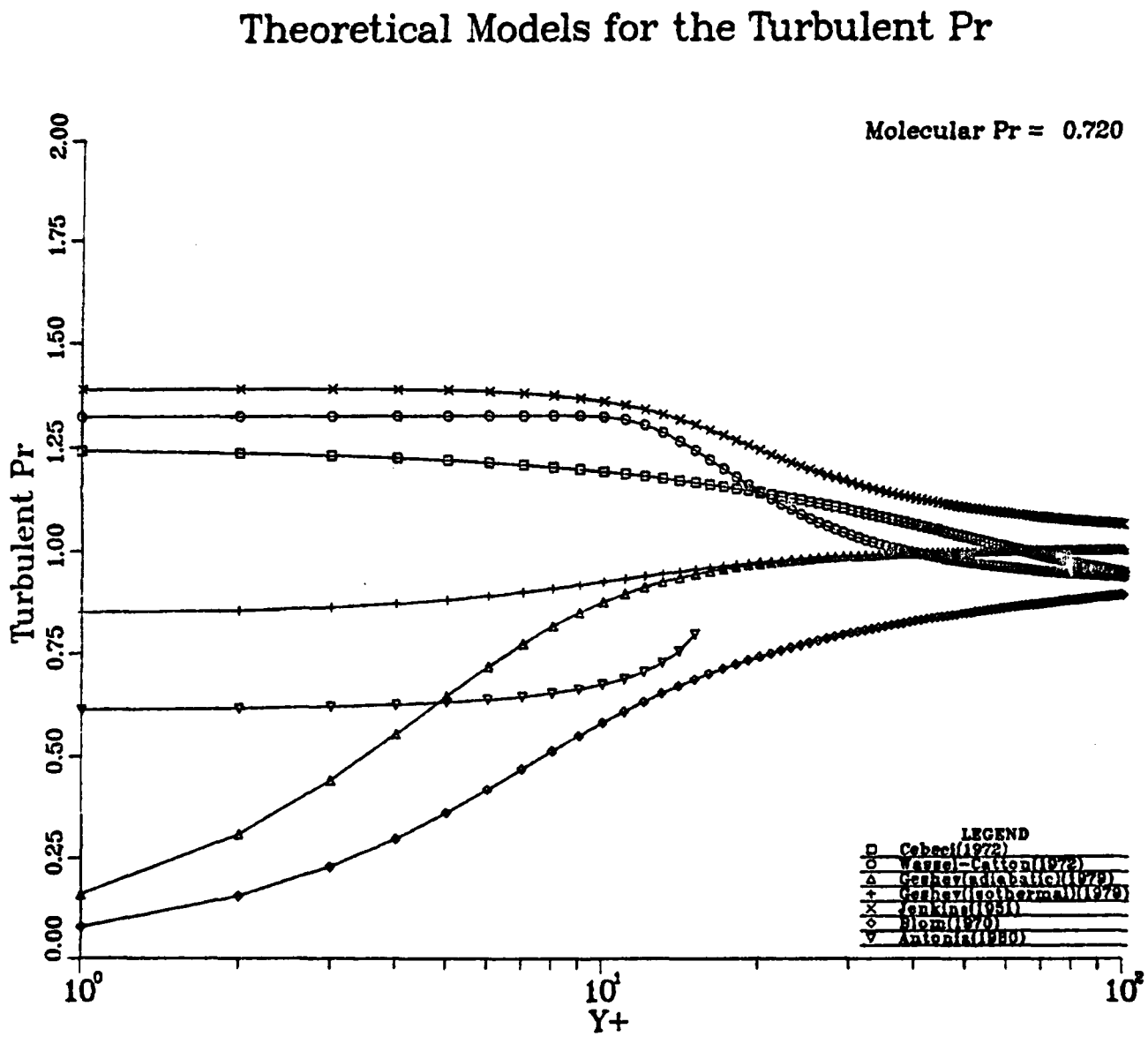

Figure 3. Some theoretical models of turbulent Prandtl number for a molecular Prandtl number of 0.72 (air).

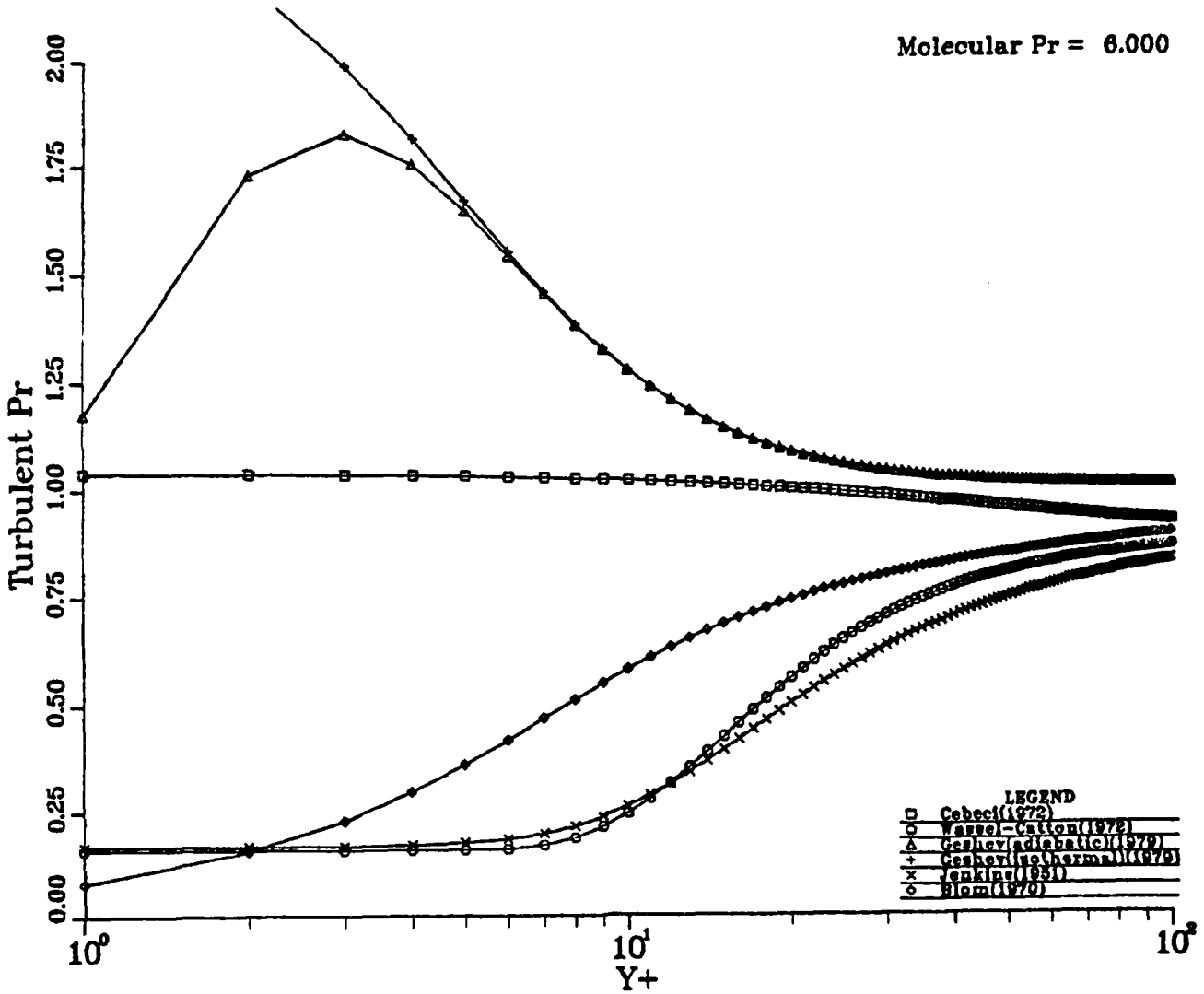

Figure 4. Some theoretical models of turbulent Prandtl number for a molecular Prandtl number of 6 (water).

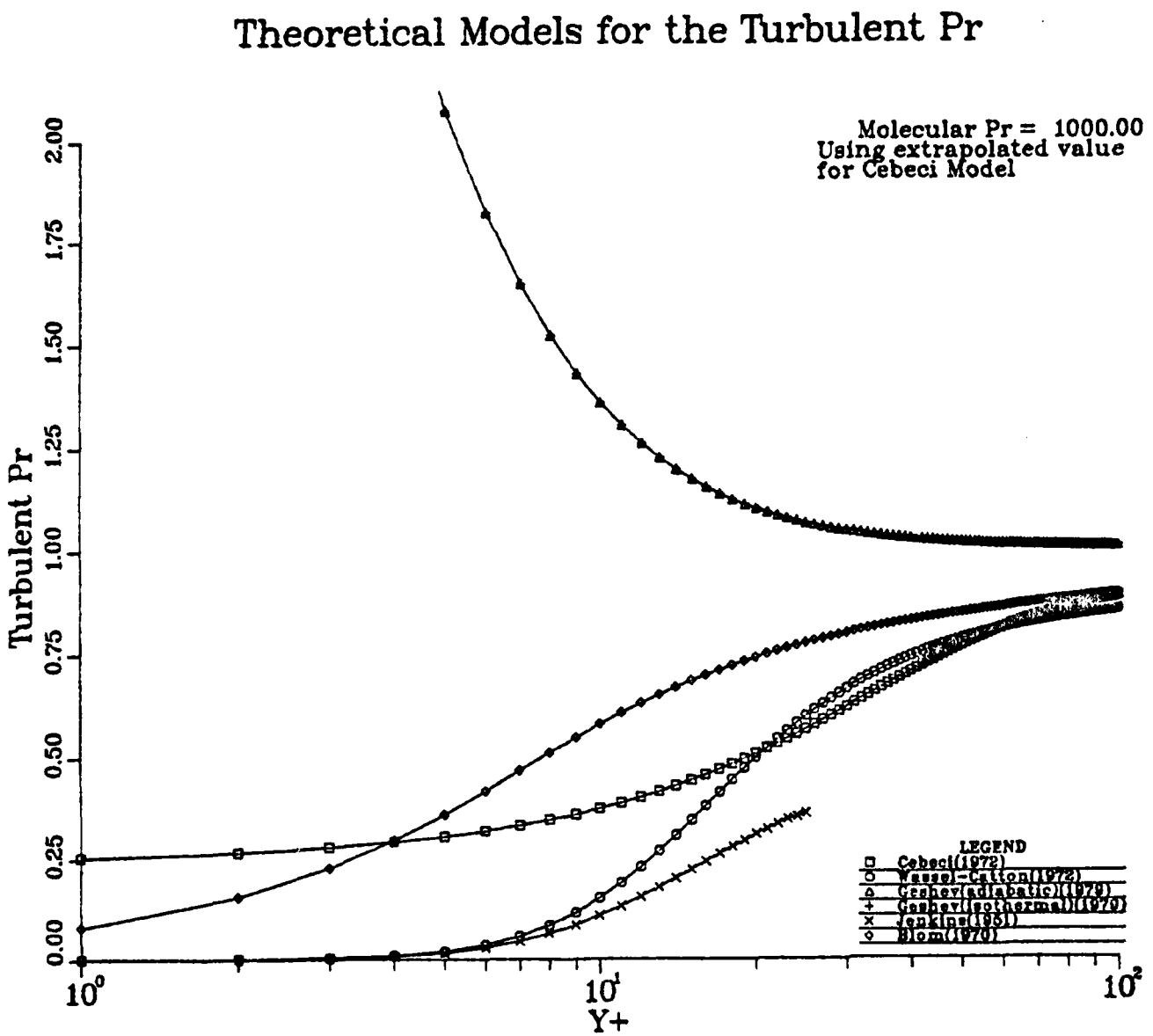

Figure 5. Some theoretical models of turbulent Prandtl number for a molecular Prandtl number of 1000 (oil).

CODE VERIFICATION

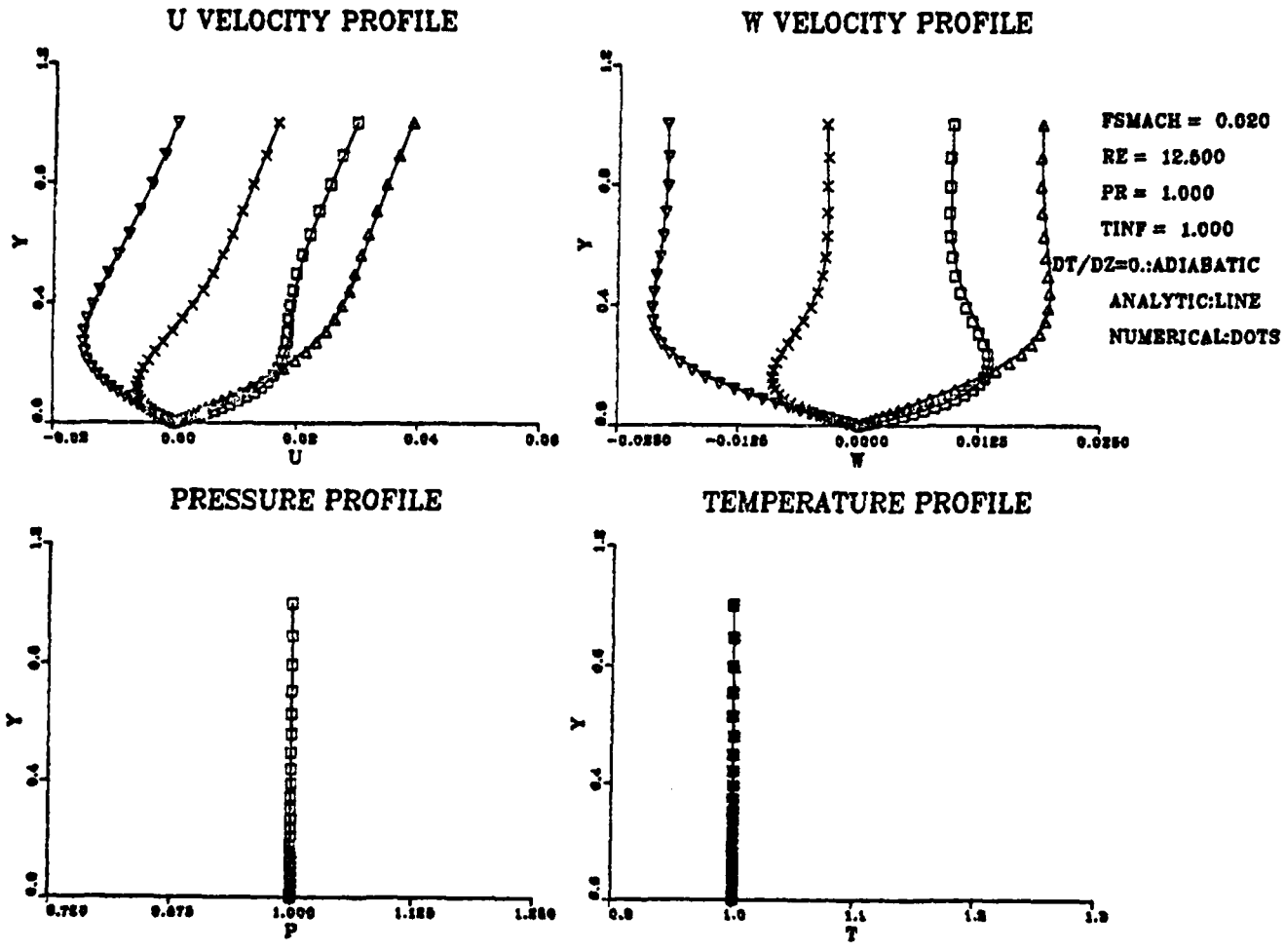

Figure 6. Comparison of numerical computations with exact analytical results for oscillating shear flow; Adiabatic wall.

CODE VERIFICATION

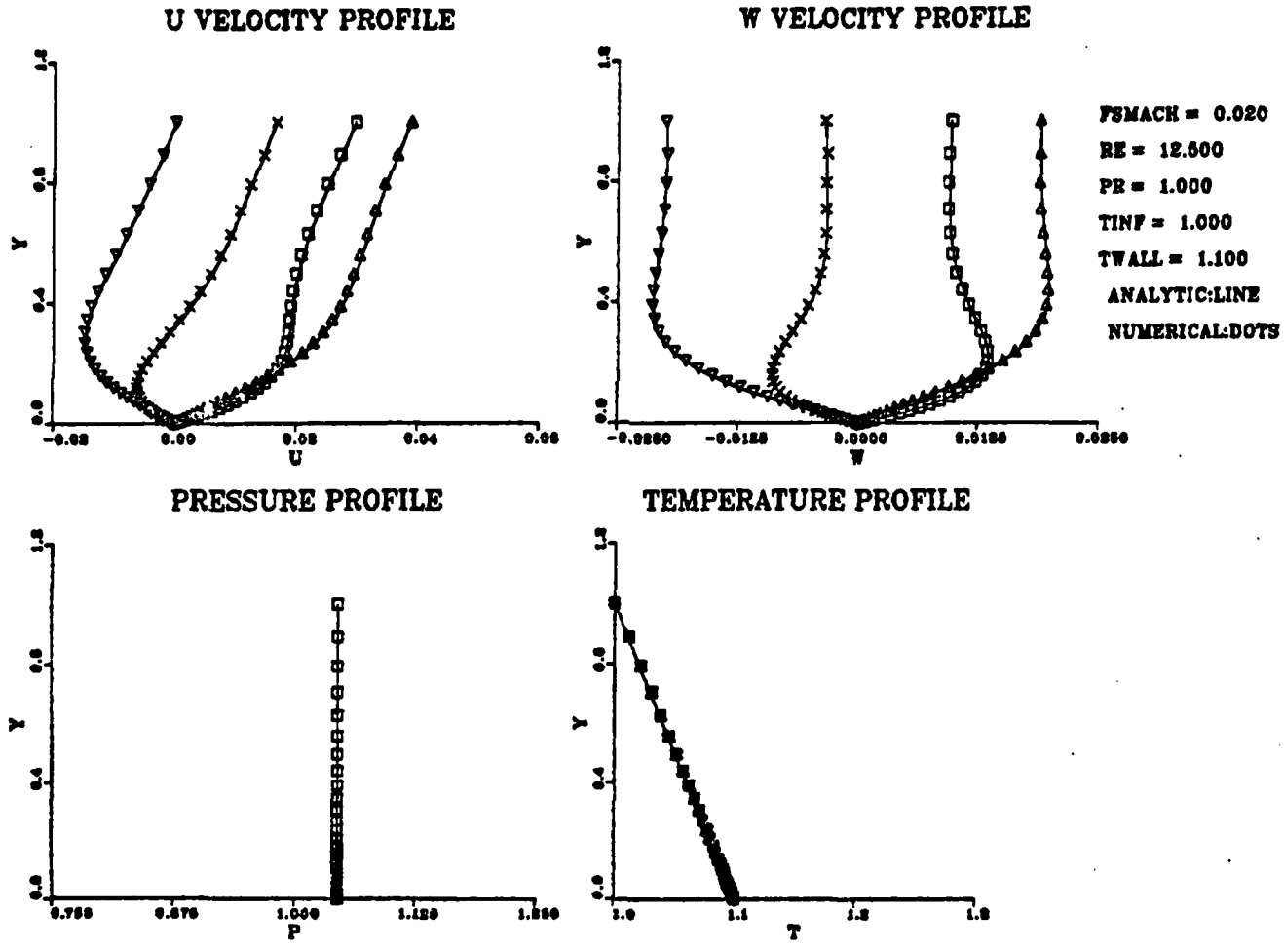

Figure 7. Comparison of numerical computations with exact analytical results for oscillating shear flow; Heat transfer case, T_w/T_∞ = 1.1.

□ Hishida,Nagano 1979
○ Subramanian,Antonia 1981
△ Back,Cuffel,Massier 1969
+ Kader 1979
× Gibson,Verriopoulous,Nagano 1980
◇ Snijders,Kopplus,Nieuwvelt 1981
▽ Johnk,Hanratty 1962
⊠ Kays,Moffat 1975
✱ Hoek,Baer 1972
◈ Elena 1976
⊖ Chen,Blackwelder 1976

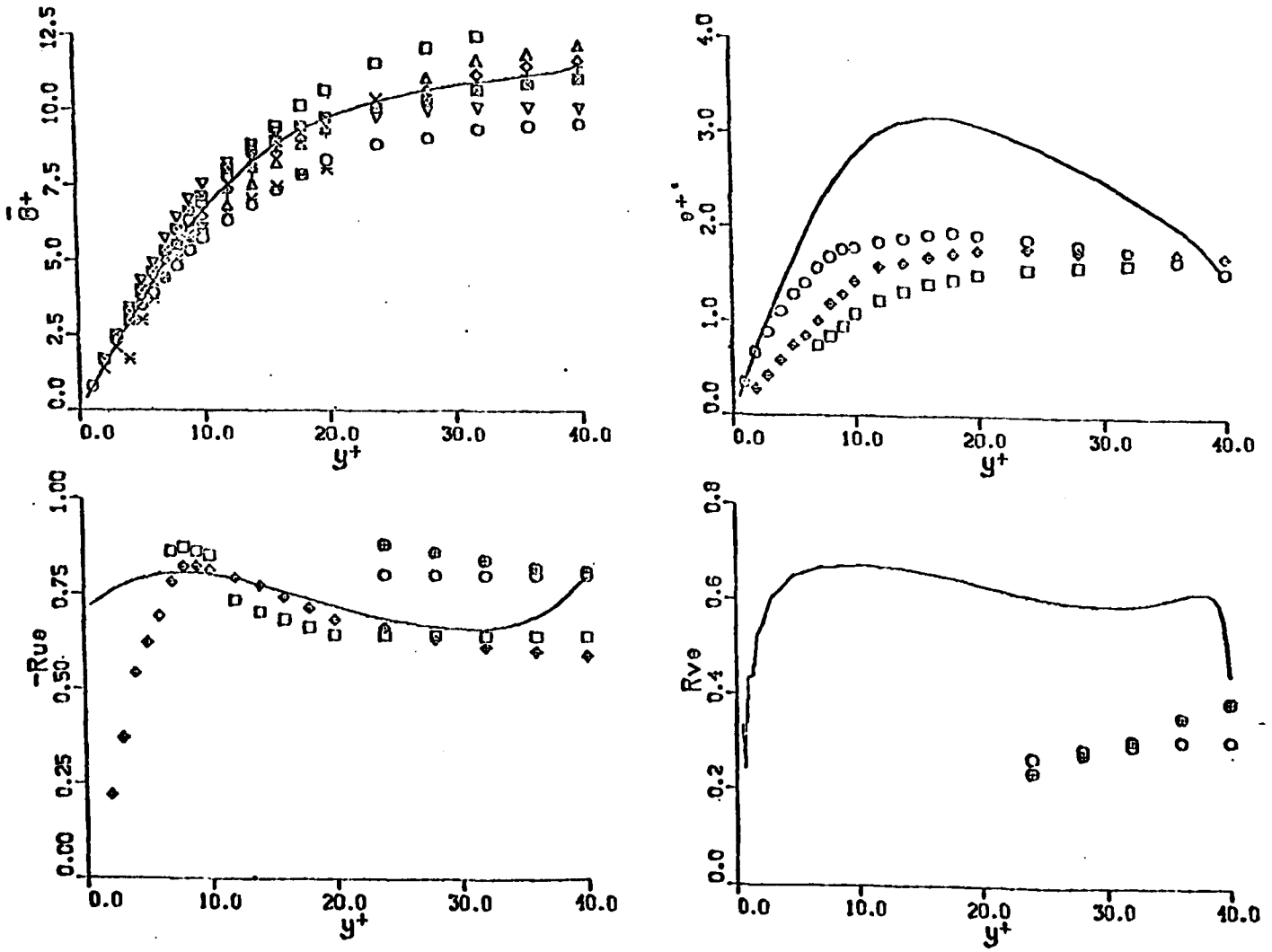

Figure 8. Comparison of preliminary computations (solid line) with experimental results for mean and fluctuating temperature, and for the temperature-velocity correlation coefficients. Molecular Pr = 0.7, zero pressure gradient.

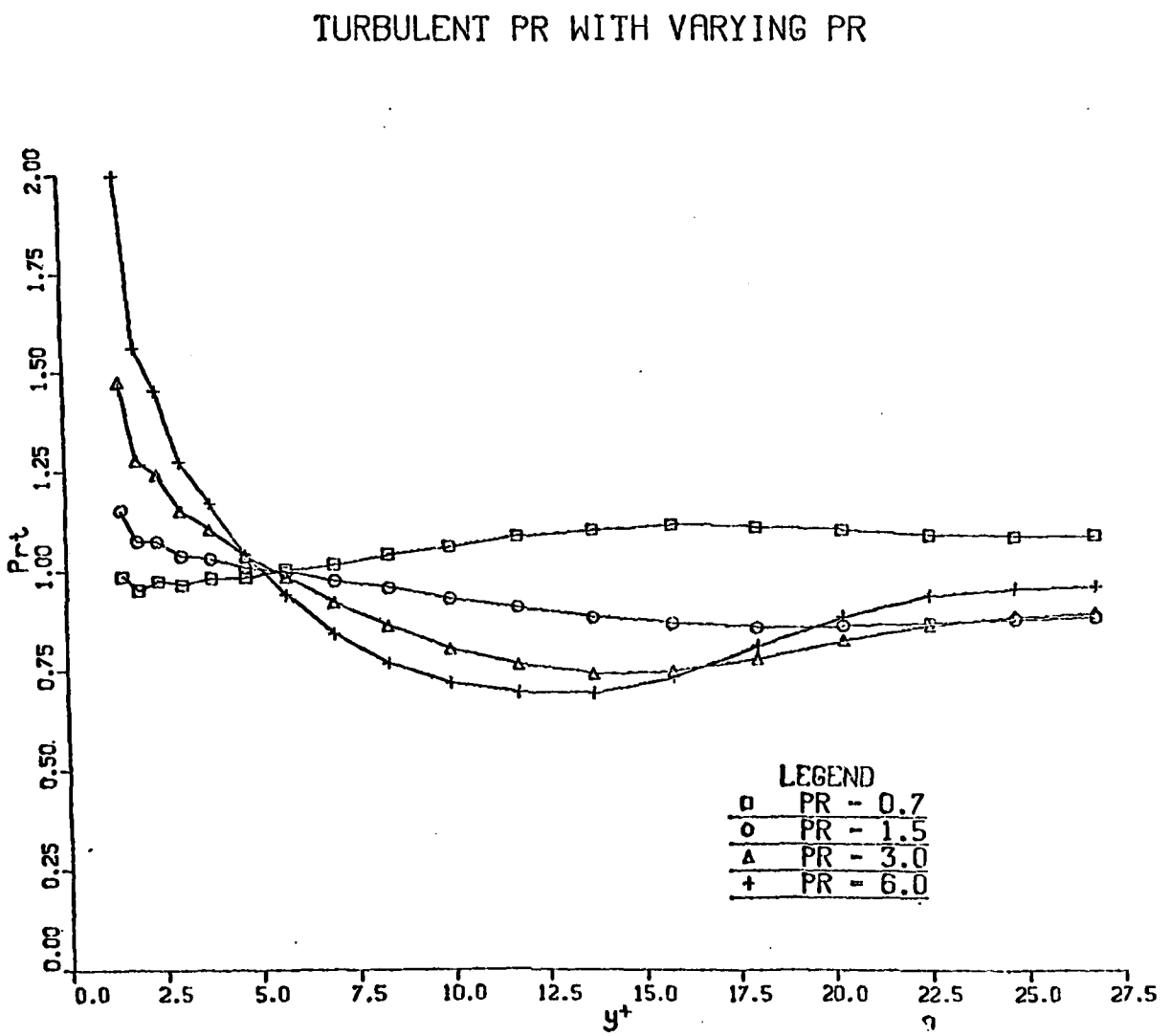

Figure 9. Preliminary computations of turbulent Prandtl number for fluids of different molecular Prandtl number. Zero pressure gradient.

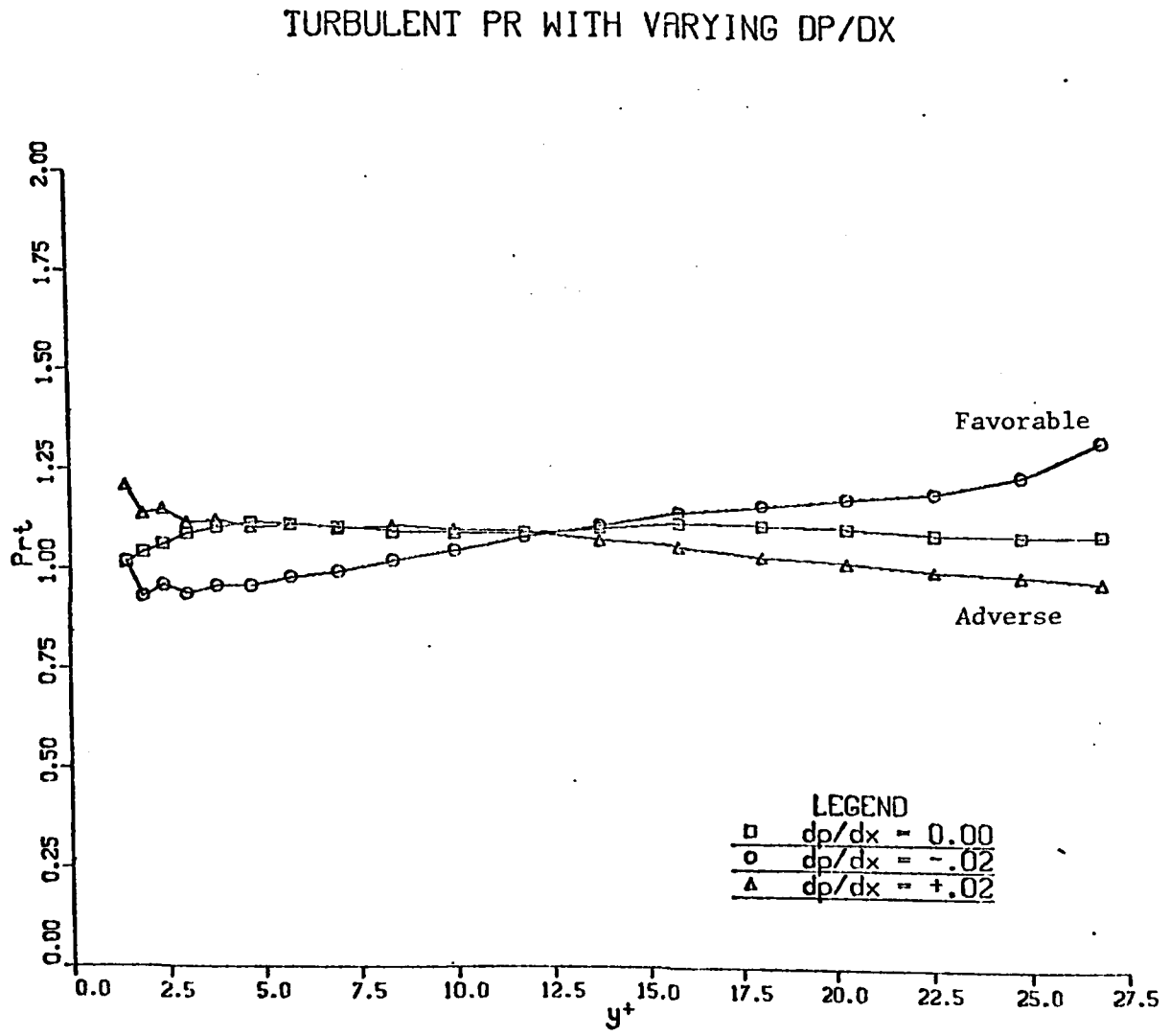

Figure 10. Preliminary computations of turbulent Prandtl number for different mean streamwise pressure gradients. Molecular Pr = 0.7, isothermal wall.

Mixture	Temperature, °F	Stress psi	Initial Strain Inches/Inch	Stiffness Modulus psi	Cycles to Failure
E	77	21.8	0.00084	25,952	4,710
		22.2	0.00059	37,627	7,620
		30.2	0.00117	25,812	2,820
		15.3	0.00037	41,351	78,300
		14.0	0.00027	51,852	56,254
		12.7	0.00020	63,500	260,277
		16.4	0.00030	54,667	83,429
		10.7	0.00069	15,507	35,135
		33.8	0.00162	20,864	2,719
		23.3	0.00097	24,021	6,550
	40	129.8	0.00039	332,821	20,461
		120.0	0.00032	375,000	30,501
		164.4	0.00047	349,787	10,493
		97.8	0.00021	465,714	113,247
		106.7	0.00032	333,438	83,394
		151.1	0.00055	274,727	8,000
		175.5	0.00081	216,667	1,632
		164.4	0.00040	411,000	5,730
		186.6	0.00074	252,162	2,400
		112.0	0.00028	400,000	109,546
F	77	21.6	0.00060	36,000	21,180
		32.4	0.00158	20,506	1,133
		16.0	0.00029	55,172	50,048
		14.0	0.00029	48,276	78,350
		18.2	0.00038	47,895	20,219
		12.7	0.00029	43,793	145,080
		20.0	0.00068	29,412	6,455
		24.0	0.00063	38,095	10,397
		26.7	0.00061	43,770	2,624
	40	133.3	0.00086	155,000	2,618
		142.2	0.00049	290,204	9,411
		164.4	0.00063	260,952	3,741
		175.5	0.00073	240,411	1,591
		111.1	0.00047	236,383	8,400
		97.8	0.00024	407,500	95,949
		122.2	0.00043	284,186	10,046
		186.6	0.00069	270,435	1,680
		120.0	0.00052	230,769	7,491
		102.2	0.00030	340,667	37,211
		96.0	0.00020	480,000	149,100

Mixture	Temperature, °F	Stress psi	Initial Strain Inches/Inch	Stiffness Modulus psi	Cycles to Failure
G	77	43.3	0.00152	24,487	998
		34.4	0.00094	36,596	2,808
		22.0	0.00063	34,921	8,250
		17.8	0.00048	37,083	16,558
		30.0	0.00095	31,579	2,472
		16.7	0.00036	46,389	64,198
		19.8	0.00071	27,887	8,460
		14.9	0.00043	34,651	27,928
		13.8	0.00029	47,586	94,024
		15.6	0.00033	47,273	68,049
	40	151.5	0.00085	178,235	675
		129.8	0.00067	193,731	1,093
		109.3	0.00042	260,238	11,680
		120.0	0.00048	250,000	4,244
		97.8	0.00039	250,769	7,263
		86.7	0.00035	247,714	17,469
		66.4	0.00030	221,333	45,166
		77.5	0.00028	276,786	43,466
		57.8	0.00023	251,304	93,982
H	77	20.0	0.00240	8,333	330
		10.7	0.00122	8,770	1,065
		8.2	0.00036	22,778	17,862
		6.7	0.00039	17,179	28,290
		5.1	0.00019	26,842	285,602
		5.8	0.00032	18,125	38,135
		5.6	0.00024	23,333	28,459
		6.7	0.00039	17,179	39,930
		7.1	0.00032	22,188	40,955
		8.4	0.00047	17,872	5,300
		8.2	0.00036	22,778	136,192
		6.7	0.00039	17,179	19,485
	40	106.2	0.00094	112,979	391
		75.5	0.00028	269,643	7,597
		54.0	0.00020	270,000	42,166
		66.7	0.00029	230,000	6,150
		50.0	0.00019	263,158	50,647
		88.9	0.00036	246,944	2,625
		46.7	0.00012	389,167	110,296
		95.5	0.00035	272,857	3,118
		102.2	0.00040	255,500	536
		46.7	0.00015	311,333	42,955

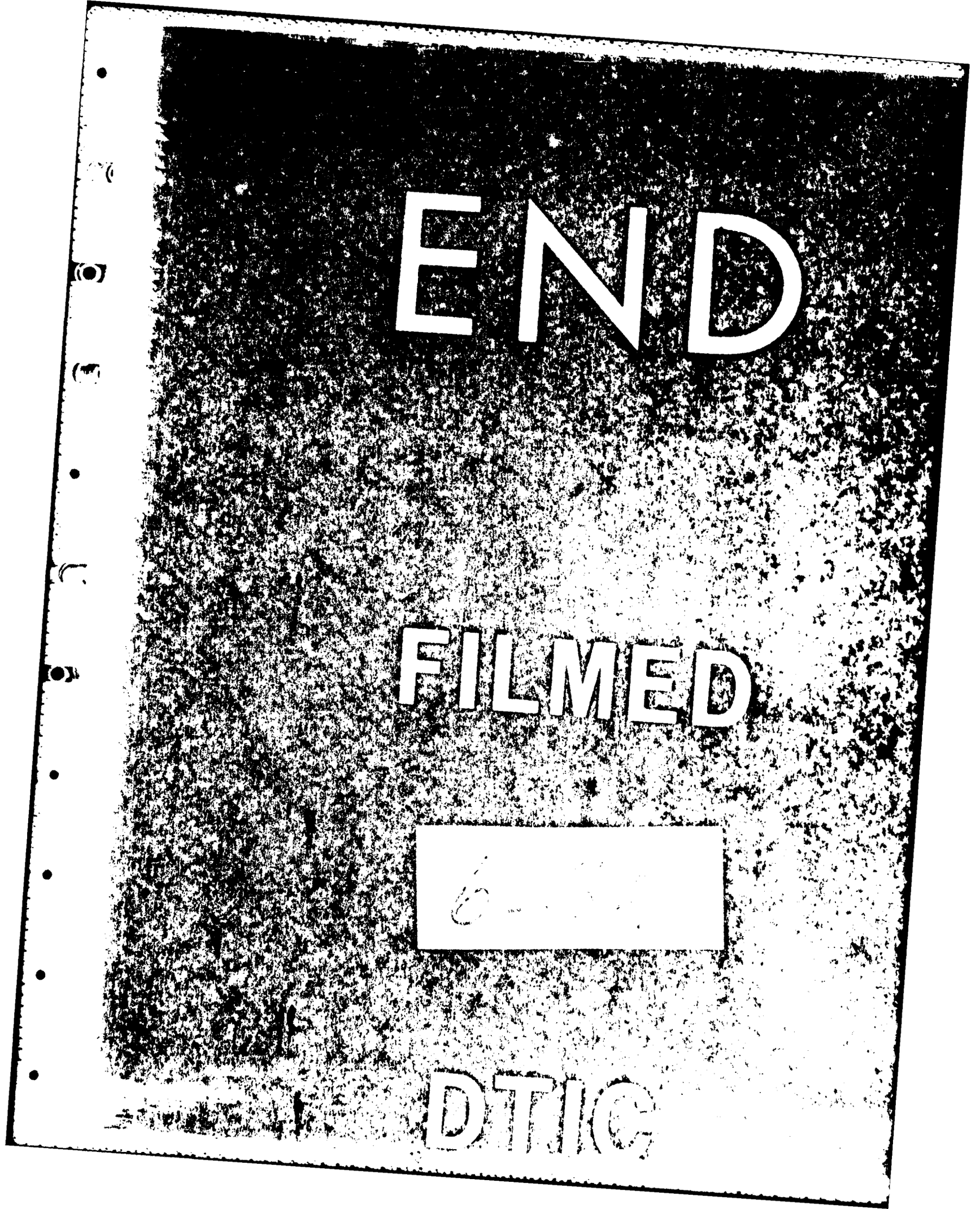
END
FILMED
DTIC